THE ASTROPHYSICAL JOURNAL, 419:494–514, 1993 December 20

THE WAVELENGTH DEPENDENCE OF POLARIZATION OF ACTIVE GALAXIES AND QUASARS

WAYNE WEBB,[1] MATTHEW MALKAN,[1] GARY SCHMIDT,[2] AND CHRIS IMPEY[2]

Received 1991 December 6; accepted 1993 June 28

ABSTRACT

We measured *UBVRI* polarizations of 0.5%–2.5% in more than a dozen "normal" quasars and Seyfert 1 galaxies. The position angle is wavelength-independent, suggesting the polarization in a given object originates in a single physical process. In many cases the percentage of polarization increases with frequency.

By fitting the multiwavelength spectra with models, we estimate the fractions of the observed flux originating in separate continuum components: infrared, recombination, stellar, and thermal. We compare the polarized fluxes observed in each filter with the predictions of competing models of polarization in AGNs: synchrotron emission, scattering from electrons or different types of dust grains, and electron scattering in an accretion flow. In nine of the sources, the polarization is best understood as scattering off dust grains. Eight of these, 0134+329 (3C 48), 0711+458 (Mrk 376), 1004+130 (4C 13.41), 1426+015 (Mrk 1383), 1534+580 (Mrk 290), 1535+547 (Mrk 486), PG 1552+08, and PG 2209+185, appear to have a nonspherical distribution of dust with grains best described by the 1977 model of Mathis, Rumpl, and Norsieck. These objects tend to be redder and, in certain cases (e.g., Mrk 486), have broad emission lines which show the same polarization as the continuum. The second most successful fit to the data assumes polarization proportional to the flux of the blue thermal component. This model best characterizes 1208+397 (NGC 4151), 2041−109 (Mrk 509), and possibly 1415+253 (NGC 5548) and 1534+580 (Mrk 290). These objects have lower levels of polarization and unpolarized (where measured) emission lines. The modest polarization associated with the thermal ultraviolet component might be due to electron scattering in an accretion disk or torus.

Subject headings: galaxies: active — galaxies: photometry — galaxies: Seyfert — polarization — quasars: general

1. INTRODUCTION

Understanding the source of the powerful continuum emission from active galactic nuclei (AGNs) has been a major goal since the discovery of quasars almost three decades ago. (We follow the usual terminology in which "quasars" and "Seyfert 1 nuclei" are two subcategories of AGNs, with relatively higher and lower luminosities, respectively). During the last decade, the continuum has been observed over a wide range of wavelengths, and researchers have concluded that more than one emission mechanism operates in the region surrounding the central engine. However, even these accumulated multiwavelength data have been insufficient to decide which mechanisms dominate in the various classes of AGNs, and how these mechanisms may be physically related. Polarization, and its wavelength dependence, is one of the less studied characteristics of the quasar central engine continuum, and it may be a key to physically distinguishing between different emission mechanisms.

Polarization in AGNs can be intrinsic or extrinsic. Intrinsic polarization is imprinted during the emission process itself. Synchrotron emission is an example of an intrinsic process, where polarization results from nonthermal emission by electrons in an anisotropic magnetic field. Extrinsic polarization is caused by a subsequent process. Scattering by a nonspherical distribution of electrons, or dust particles, near the central engine, or by magnetically aligned dust grains in the interstellar medium of the galaxy, are examples of proposed extrinsic polarization mechanisms. The resulting wavelength dependence of polarization is unique to each of these mechanisms, making multiwavelength polarimetry a potentially powerful diagnostic tool.

While the origin of polarization is not known for the vast majority of optically selected low-polarization quasars, it is believed to be understood for blazars and Seyfert 2 galaxies. In the former, a synchrotron jet (probably beamed) emits highly polarized and violently variable radio and optical continua. Radio quasars with compact cores are observed to have high optical polarization ($P \geq 3\%$), rapid optical variability of large amplitude, featureless red continua, and apparent superluminal motion of VLBI radio components (Stockman, Moore and Angel 1984 [SMA]; Impey 1987). In Seyfert 2 galaxies, polarization appears to arise from scattering of the light of an otherwise obscured active nucleus.

There may also be a distinction in the polarization mechanisms of high- and low-luminosity AGNs. For example, the correlation between the polarization position angle and the symmetry axes of some Seyfert galaxies (Thompson & Martin 1988) implies that the polarization arises from transmission by aligned dust grains far from the central engine. Higher luminosity quasars are less likely than Seyfert galaxies to have $P > 2\%$, and the source of the polarization is more uncertain, at least for the majority of them which lack strong radio cores and violent variability.

Polarimetric studies of AGNs usually rely on one of two approaches. One can observe the white-light polarizations of

[1] Department of Astronomy, University of California, Los Angeles, CA 90024.
[2] Steward Observatory, University of Arizona, Tucson, AZ 85721.

many members of a class of AGNs. Correlating polarization statistics with other observables may allow one to infer the polarization and emission mechanisms. For example, the polarization in some Seyfert galaxies correlates with measures of dust in the narrow line region, suggesting polarization by dust scattering (Berriman 1989). Alternatively, the correlation between compactness of the radio source and variability of polarization in radio-loud quasars is interpreted as evidence for polarization by the synchrotron process (Impey & Tapia 1989). A second approach is to study the polarization of individual AGNs at spectral resolution sufficient to resolve emission lines. This is usually possible only for the brighter and more strongly polarized objects in a class (e.g., NGC 4151 [Schmidt & Miller 1980] and NGC 1068 [Antonucci & Miller 1985]).

In this paper we take a third, intermediate approach in which we collect and analyze low spectral resolution (broadband) polarimetry on more than a dozen AGNs. In order to obtain signal-to-noise ratios $[P/\sigma(P)]$ of order 10 on low-polarization quasars (LPQs) and Seyfert galaxies, the targets should be brighter than $m_b \sim 16$. Even these bright sources may have such small polarizations (less than one-half of 1%) that adequate signal-to-noise cannot be achieved in any practical integration time. We measure the spectral shape of continuum polarization in several broad spectral bands and correlate it with other observables of the AGNs.

2. MEASUREMENT OF THE WAVELENGTH DEPENDENCE OF POLARIZATION

2.1. *Object Selection*

The objects included in this study were chosen from two large surveys of the white-light polarizations of quasars (Berriman et al. 1990 and SMA) to (1) have significant ($\geq 1\%$) optical polarization, yet not be known OVVs, (2) be bright enough that accurate *UBVRI* polarimetry was practical, (3) cover a range of luminosities and object types, (4) have relatively blue colors, thereby minimizing internal reddening, and (5) be at high Galactic latitudes, thereby avoiding significant polarization due to interstellar material in our Galaxy.

Table 1 lists the 26 high-luminosity Seyfert 1 galaxies, optically selected quasars, and radio-selected quasars, originally in our polarimetry program. Three objects for which multiwavelength polarimetry has been published are noted. These are low-luminosity Seyfert 1 galaxies observed by Thompson et al. (1979), Schmidt & Miller (1985), and Antonucci (1984). Published measurements of some of these objects will be used to augment our data and serve as "template" systems to validate our polarization models. For nine of our program objects we have polarimetry in only one or two wavebands, and for two objects continuum flux measurements are incomplete. This leaves a total of 15 AGNs with sufficient multiwavelength data for our complete analysis.

TABLE 1

POLARIMETRY PROGRAM QUASARS

Object	Type[a]	z	Log F[b] (mJy)	M_B	E_{B-V} (Internal)	Stars[c] (mJy)[b]	References
0050+124 (PG, I Zw 1)	S/Q	0.060	0.83	−22.55	0.06	1.40	1, 5
0134+329 (3C 48)	R	0.367	0.05	−24.40	0.03	0.10	6
0349−146 (3C 95)[d]	R	0.614	...	−25.79	...	...	...
0405−123 (Pks)[d]	R	0.574	...	−27.34	...	...	...
0414−06 (Pks, 3C 110)	R	0.781	−0.04	−26.62	0.00	0.02	7
0711+458 (Mrk 376)[e]	S	0.056	0.63	−21.57	0.10	1.60	1, 8
0923+129 (Mrk 705)[d]	S/Q	0.029	...	−20.39	...	...	...
1001+054 (PG)[d]	Q	0.161	...	−22.91	...	...	...
1004+130 (PG, 4C 13.41)	R	0.240	0.47	−23.98	0.03	0.05	6
1012+01 (PG)[d]	Q	0.185	...	−23.45	...	...	...
1048−09 (PG, 3C 246)[f]	R	0.344	...	−24.69	...	...	...
1114+445 (PG)	Q	0.089	0.27	−22.75	0.00	0.50	9
1138+04 (PG)[d]	Q	1.876	...	−28.25	...	...	...
1151+117 (PG)[d]	Q	0.176	0.10	−23.73	0.00	0.16	9
1208+397 (NGC 4151)[e]	S	0.003	1.63	−18.31	0.00	7.00	2, 5
1216+07 (PG)[d]	Q	0.334	...	−24.94	...	...	...
1222+228 (PG, Ton 1530)	Q	2.05	0.07	−28.99	0.00	0.00	10, 9
1254+047 (PG)[f]	Q	1.024	...	−27.19	...	...	...
1415+253 (NGC 5548)[e]	S	0.017	1.12	−19.80	0.02	3.00	2, 5
1426+015 (Mrk 1383)	S/Q	0.086	0.78	−22.63	0.00	0.68	1, 9
1501+106 (Mrk 841)[d]	S/Q	0.036	...	−20.70	...	...	...
1534+580 (PG, Mrk 290)	S/Q	0.031	0.60	−19.86	0.00	1.10	1, 8
1535+547 (Mrk 486)	S/Q	0.039	0.61	−20.60	0.05	0.50	1, 4, 8
1552+08 (PG)	Q	0.119	0.28	−22.37	0.00	0.36	9
2041−109 (Mrk 509)[e]	S	0.035	1.11	−22.39	0.00	1.50	2, 5
2209+185 (PG)	Q	0.070	0.56	−21.38	0.00	1.00	4, 7, 9

REFERENCES.—(1) Unpublished data from Palomar 60 inch. (2) Malkan & Filippenko 1983. (3) Hutchings et al. 1984. (4) Neugebauer et al. 1985. (5) Edelson & Malkan 1986. (6) Neugebauer et al. 1979. (7) Unpublished data from Lick Observatory. (8) de Bruyn & Sargent 1978. (9) Neugebauer et al. 1987. (10) Inferred from high redshift and extremely high luminosity.

[a] Type: Q = radio-quiet quasar, R = radio-loud quasar, S = Seyfert galaxy.

[b] Log flux at log $\nu = 14.74$. Luminosities for $H_0 = 75$ km s^{-1} Mpc^{-1}.

[c] Flux density at 5500 Å in 10″ aperture.

[d] Polarimetry in two or fewer bands.

[e] Previously published multiwavelength polarimetry.

[f] UV and optical continuum mismatch.

2.2. *Observations*

The data were obtained with two polarimeters. Both instruments achieve polarimetric modulation by means of a rotating achromatic half-wave retarder under continuous computer control. Guiding was performed with an intensified acquisition TV. Northern hemisphere objects were observed primarily with the "Two-Holer" polarimeter on the 2.3 m telescope of Steward Observatory during the period from 1982 May to 1986 September. Supplementary observations utilized the 1.5 m telescope at Mt. Lemmon and the 5 m Hale telescope. Spectral bandpasses were defined by colored glass filters which closely resemble the Kron-Cousins *UBVRI* filter system (3250–3900, 3800–4800, 5000–6100, 5600–7200, and 7250–8600 Å, respectively, where limits refer to half-power points). These fixed bandpasses may not be optimal for the spectrum of any particular active galaxy, but characterize the shape of the polarization spectrum in a reasonable allotment of telescope time. In some instances the combined white (W)–light polarizations were measured. The unfiltered W band was limited only by the atmospheric cutoff in the UV (3200 Å) and the falloff of instrumental sensitivity in the red (approximately 8600 Å).

In the southern hemisphere, observations were made with the "MINIPOL" polarimeter on the du Pont 2.5 m telescope at Las Campanas Observatory during the period 1984 March–1986 May. Like "Two Holer," MINIPOL has low instrumental polarization ($P \leq 0.01\%$), and fast polarimetric modulation so that the quality of the data is not affected by minor variations in atmospheric transparency. For observations of bright AGNs, the accuracy of the polarimetry is determined primarily by photon statistics. The precision of MINIPOL, and the reliability of measurements in low polarization for faint extragalactic objects, is discussed by Impey, Malkan & Tapia (1989).

The data were acquired and reduced in standard fashion. All of the polarimetry was obtained with a 2".7 aperture, except for six measurements (indicated in Table 2) taken with a 5".4 aperture, using frequent observations of the background sky through telescope offsets. The degree of polarization was calibrated with measurements of bright comparison stars through a fully polarizing prism, and position angles were rectified to the equatorial system by means of measurements of interstellar polarization standards obtained each observing run.

2.3. *Results*

Since the typical interstellar polarization has a maximum (usually in the visual) of $P_{\max} = 4\%$–9% of $E_{(B-V)}$, the expected interstellar polarizations for most of the program quasars are of order 0.1%. In five cases we measured the interstellar polarization directly by observing two or three field stars near the program quasars 1004+130, 1222+228, 1254+047, 1426+015, and 1552+08 (Table 2). These corrections were generally small and were not subtracted from that of the AGNs.

Our polarimetry measurements for all of the objects are presented in Table 2. Multiple measurements were averaged in Stokes-parameter space for each object, resulting in a mean polarimetric signal to noise ratio of order 10 in each spectral band. In Table 3 the average polarizations are summarized for the 13 objects for which we have the best wavelength coverage. To extend our analysis to a broader quasar sample for statistical purposes, we also consider several wavelength-dependent polarization measurements published in the literature. These include NGC 4151 (Schmidt & Miller 1985), Mrk 376 (Martin et al. 1982), and Mrk 509 and NGC 5548 (Thompson & Martin 1988).

Corrections (a slight decrease) to the time-averaged polarizations were computed for the bias which is present in the noisy measurements of a positive definite quantity such as P. These "most likely" polarizations were calculated statistically in the manner of Wardle & Kronberg (1974). In Figures 3*a*–3*p*, which compare polarization models, the observed polarizations are corrected for this bias.

We compared our broad-band filter polarimetry with the measurements obtained by Martin et al. (1983) and with spectropolarimetry published by Schmidt & Miller (1985). Within the measurement uncertainties, the polarizations and position angles agree at each wavelength. The magnitude of polarization we observed is also consistent with the white-light polarizations measured by SMA and others. We find no evidence for temporal variability in the amounts of polarization or in the position angles of any of the sources studied here.

In Table 3 we also introduce polarized fluxes and characterize the general shape of the polarization spectrum with the parameter "b" determined by a least-squares fit proportional to $P_\nu F_\nu = A\nu^{+b}$. We find the slope of the wavelength dependence of polarized flux varies widely, between -2 and $+1$, with a typical uncertainty of 0.3.

Our observations often show an increase in percentage of polarization toward shorter wavelengths. The measured position angles (P.A.) are constant (wavelength-independent) for most objects, suggesting that the polarization is dominated by a single source with a specific geometry. Possible exceptions to this rule are I Zw 1, 1004+13, and 2209+185 where the *I*-band (and less noticeably the *R*) polarization vectors appear rotated from the position angles of all other bands. When a simple linear least-squares fit is made to the position angle as a function of wavelength, we find for I Zw 1: P.A. = $31 - 0.00307\lambda(\text{Å})$ degrees. The fitting uncertainty on the slope coefficient is 0.0013, indicating that the data are inconsistent with a constant position angle (zero slope) at only the 2.2 σ level.

3. CONTINUUM FITTING OF THE DATA

3.1. *Continuum Components*

The continuum emission observed from AGNs is believed to originate from more than one physical mechanism, possibly in more than one site in and around the central engine. Unfortunately, we do not know a priori which continuum components are polarized, or in what way. To make progress, and to test specific hypotheses, we need to compare the observed wavelength dependence of polarization with predictions which depend upon the relative strengths of the different continuum components. An accurate estimate of these components requires measurements over a wide range of wavelengths. For all but two of the AGNs for which we have multiwavelength polarimetry, we were able to construct continuum energy distributions from the ultraviolet (measured by the *International Ultraviolet Explorer*, 0.1–0.3 μm) to the near-, or even mid-infrared (greater than 10 μm). For completeness, *IRAS* detections were included when available, although it is unclear how much of the far-infrared flux is emitted by the nucleus.

In Figures 1*a*–1*o* we display the continuum observations with errors bars for 15 of these sources. A description of the multicomponent model fit to the spectra, represented by the solid lines, is given in § 3.2. Corrections have been made for

TABLE 2

MEASUREMENT DATA: *UBVRI* AND W POLARIZATIONS, POSITION ANGLES, AND STANDARD DEVIATIONS[a]

AGN	Date	*U*	*B*	*V*	*R*	*I*
PG 0050+124 (I Zw 1)	1983 Sep 02	...	1.14 ± 0.08	0.65 ± 0.06	0.38 ± 0.07	0.26 ± 0.09
		...	15.4 ± 1.9	17.1 ± 2.6	8.8 ± 5.0	169.4 ± 9.6
	1983 Dec 08	1.70 ± 0.20	...	...	...	0.31 ± 0.11
		19.8 ± 3.3	...	...	...	1.9 ± 9.7
	1983 Dec 12	...	...	...	...	0.28 ± 0.07
		...	...	...	...	8.2 ± 6.9
	1983 Dec 13	...	...	...	0.36 ± 0.07	...
		...	...	...	22.4 ± 6.1	...
	1982 Dec 14	...	White (W):	0.61 ± 0.08	...	...
		...	...	8.4 ± 2.9	...	...
0134+329 (3C 48)	1984 Oct 05	1.68 ± 0.21	1.74 ± 0.19	1.58 ± 0.14	1.22 ± 0.13	1.08 ± 0.13
		150.8 ± 3.6	161.4 ± 3.1	161.9 ± 2.5	158.9 ± 3.0	159.8 ± 3.3
	1984 Oct 28	...	2.35 ± 0.29	1.17 ± 0.42	1.62 ± 0.59	0.93 ± 0.61
		...	163.5 ± 3.5	172.8 ± 10.2	171.3 ± 10.5	130.4 ± 19.0
	1984 Oct 29	...	...	1.02 ± 0.34	1.04 ± 0.27	0.06 ± 0.49
		...	...	168.9 ± 9.5	163.7 ± 7.4	168.8 ± —
	1985 Jan 21	2.53 ± 0.59	...	White (W):	1.07 ± 0.31	...
		173.2 ± 6.6	...	...	162.8 ± 8.2	...
0349−146 (3C 95)	1984 Mar 25	...	0.65 ± 0.35	...	...	
		...	142 ± 15	...	...	...
Pks 0405−123	1984 Mar 23	...	0.22 ± 0.08[b]	...	...	...
		...	25. ± 10.	...	...	...
Pks 0414−06 (3C 110)	1984 Oct 3	0.81 ± 0.16	1.06 ± 0.18	...	...	...
		137.3 ± 6.1	132.9 ± 4.9	...	...	...
	1984 Mar 24	...	0.66 ± 0.24	...	...	...
		...	155. ± 10.	...	...	...
		...	...	White:	0.73 ± 0.31	...
		...	...	...	133.3 ± 11.8	...
	1984 Oct 04	...	...	1.06 ± 0.46	...	...
		...	...	154.0 ± 12.4	...	...
	1984 Oct 05	...	...	0.89 ± 0.17	1.04 ± 0.17	...
		...	...	147.2 ± 5.4	146.7 ± 4.7	...
	1984 Oct 29	...	...	...	...	0.70 ± 0.39
		...	...	...	...	155.9 ± 16.0
0923+129 (Mrk 705)	1984 Mar 25	...	0.47 ± 0.10	...	...	...
		...	146 ± 6	...	...	...
PG 1001+054	1984 Mar 24	...	0.31 ± 0.23	...	...	...
		...	85 ± 20	...	...	...
1004+130 (4C 13.41)[c]	1984 Mar 23	1.64 ± 0.17[b]	1.13 ± 0.13[b]	...	...	0.71 ± 0.15[b]
		57. ± 3.	58. ± 3.	...	...	24. ± 6.
	1984 Mar 24	...	...	1.43 ± 0.14	0.90 ± 0.12	...
		...	...	63. ± 3.	43. ± 4.	...
PG 1012+01	1984 Mar 25	...	0.39 ± 0.11	...	...	...
		...	105. ± 8	...	...	...
PG 1048−09 (3C 246)	1984 Mar 24	...	1.05 ± 0.22	...	...	...
		...	59 ± 6	...	...	...
	1985 Apr 12	...	0.83 ± 0.25	...	1.47 ± 0.15	1.86 ± 0.78
		...	100. ± 9.	...	102. ± 3.	77. ± 12.
	1985 Apr 13	0.79 ± 0.78	...	...	...	1.79 ± 0.96
		105. ± 17.	...	...	...	96. ± 16.
PG 1114+445	1983 Mar 10	White (W):	2.37 ± 0.18	...	...	...
		...	96.5 ± 2.2	...	...	...
	1984 Jan 09	...	...	2.27 ± 0.43	3.28 ± 0.40	2.17 ± 0.35
		...	...	90.3 ± 5.5	85.2 ± 3.5	102.2 ± 4.6
	1984 Jan 10	...	2.97 ± 0.44	1.67 ± 0.33	1.78 ± 0.35	1.75 ± 0.40
		...	99.7 ± 4.2	97.7 ± 5.7	88.1 ± 5.5	86.1 ± 6.5
	1984 Mar 04	2.69 ± 0.30	2.91 ± 0.31	2.10 ± 0.26	1.93 ± 0.23	2.18 ± 0.25
		105.4 ± 3.2	100.2 ± 3.0	94.8 ± 3.5	96.0 ± 3.4	97.3 ± 3.3
PG 1138+04	1984 Mar 23	...	0.85 ± 0.19	...	...	...
		...	48 ± 6	...	...	...
PG 1151+117	1984 Mar 24	...	...	...	...	0.98 ± 0.54[b]
		...	...	...	...	137. ± 18.
	1984 Mar 25	...	0.67 ± 0.13	...	...	...
		...	155. ± 5.6	...	...	...
PG 1216+07	1984 Mar 26	...	0.44 ± 0.21	...	...	...
		...	13. ± 14.	...	...	...

TABLE 2—*Continued*

AGN	Date	*U*	*B*	*V*	*R*	*I*
1222+228 (Ton 1530)[d]	1984 Mar 23	...	...	...	...	0.91 ± 0.46
		...	...	...	...	134. ± 14.
	1984 Mar 25	...	0.66 ± 0.17	...	...	0.62 ± 0.62
		...	120.7 ± 7.	...	...	144. ± 29.
	1984 Mar 26	...	...	...	...	0.74 ± 0.27
		...	...	...	...	134. ± 10.
	1984 Mar 27	...	...	...	0.67 ± 0.29	...
		...	...	...	149. ± 12.4	...
		...	...	...	0.96 ± 0.27	...
		...	...	...	146. ± 8.	...
	1984 Mar 28	...	0.67 ± 0.29	...	...	...
		...	149 ± 12.	...	...	...
	1985 Apr 16	2.56 ± 1.43	...	...	...	...
		34. ± 15.	...	...	...	...
PG 1254+047	1984 Mar 26	...	1.22 ± 0.19	...	1.63 ± 0.26	1.98 ± 0.87
		...	170. ± 4.	...	3. ± 5.	12. ± 13.
	1984 Mar 28	0.89 ± 0.34	...	...	...	...
		6. ± 11.	...	...	...	...
1426+015 (Mrk 1383)[f]	1984 Mar 23	...	...	...	...	0.68 ± 0.19
		...	...	...	...	74. ± 8.0
	1984 Mar 24	...	0.84 ± 0.10	0.76 ± 0.10	...	...
		...	79. ± 3.	78. ± 4.	...	...
	1984 Mar 25	0.85 ± 0.11	...	...	...	0.46 ± 0.13
		84. ± 4.	...	...	...	89. ± 8.1
1501+106 (Mrk 841)	1984 Mar 22	...	...	...	...	0.42 ± 0.10[b]
		...	...	...	...	104. ± 7.
1534+580 (Mrk 290)	1980 Mar 16	...	White (W):	0.79 ± 0.14	...	...
		...	...	137.6 ± 5.2	...	...
	1984 Mar 04	1.46 ± 0.29	1.22 ± 0.18	0.95 ± 0.12	0.68 ± 0.11	0.52 ± 0.13
		142.9 ± 5.6	146.7 ± 4.2	148.3 ± 3.7	147.5 ± 4.6	145.3 ± 7.0
1535+547 (Mrk 486)	1980 Mar 16	...	White (W):	2.48 ± 0.12	...	...
		...	...	133.3 ± 1.3	...	...
	1982 Apr 21	3.63 ± 1.00	...	...	...	7.44 ± 2.70
		148.1 ± 6.7	...	...	...	145.8 ± 10.6
	1982 May 30	4.46 ± 0.90	...	...	...	2.61 ± 0.94
		161.3 ± 5.8	...	...	...	140.9 ± 10.4
	1982 Sep 22	3.04 ± 1.36	...	...	...	2.75 ± 0.41
		142.8 ± 9.0	...	...	...	144.2 ± 4.3
	1983 Mar 31	3.59 ± 0.55	...	...	...	2.07 ± 0.29
		139.7 ± 4.4	...	...	...	141.7 ± 3.9
	1983 Aug 30	...	2.85 ± 0.30	2.46 ± 0.17	2.10 ± 0.15	2.46 ± 0.19
		...	145.2 ± 3.0	144.1 ± 2.0	138.0 ± 2.1	147.0 ± 2.2
	1983 Sep 02	...	3.49 ± 0.24	2.94 ± 0.26	2.11 ± 0.17	2.03 ± 0.24
		...	134.9 ± 2.0	139.9 ± 2.5	139.9 ± 2.3	136.6 ± 3.3
	1984 Mar 03	3.90 ± 0.27	...	...	...	...
		140.3 ± 2.0	...	...	...	...
PG 1552+08[a]	1984 Mar 27	3.07 ± 0.58	...	...	...	1.31 ± 0.31
		69. ± 5.4	...	...	...	78. ± 6.8
	1984 Mar 26	...	1.96 ± 0.18	...	...	...
		...	88. ± 2.6	...	...	...
	1984 Mar 28	...	...	...	1.32 ± 0.18	...
		...	...	...	76. ± 3.9	...
PG 2209+185	1980 Jun 19	...	...	White (W):	1.21 ± 0.28	...
		...	...	...	23.7 ± 6.6	...
	1983 Aug 30	...	...	0.46 ± 0.27	...	0.68 ± 0.26
		...	27.7 ± 16.8	...	67.9 ± 10.9	
	1983 Aug 31	...	1.18 ± 0.70	...	0.46 ± 0.19	...
		...	177.3 ± 17.0	...	16.4 ± 12.0	...
	1983 Sep 02	...	0.89 ± 0.44	0.44 ± 0.23	0.35 ± 0.21	0.48 ± 0.22
		...	20.3 ± 14.0	166.5 ± 14.7	165.0 ± 17.0	19.8 ± 14.4
	1983 Dec 13	...	...	...	...	0.13 ± 0.35
		...	...	...	...	12.0 ± –

[a] Polarization (%)/Position Angle (degree).
[b] 5″4 aperture.
[c] Field star polarimetry (direction from AGN: % P, P.A.). Southwest: 0.26 ± 0.04, 95. ± 4.4. Northeast: 0.23 ± 0.06, 71. ± 7.5. South: 0.15 ± 0.07, 85. ± 14.
[d] Field star polarimetry. Southwest: 0.24 ± 0.01, 49. ± 1.2. West: 0.12 ± 0.04, 84. ± 9.6. Far West: 0.61 ± 0.05, 118. ± 2.3.
[e] Field star polarimetry. South Southwest: 0.33 ± 0.06, 66. ± 5.2. Southeast: 0.19 ± 0.04, 64. ± 6.0.
[f] Field star polarimetry. "A": 0.28 ± 0.05, 60. ± 5.1. "B": 0.18 ± 0.03, 75. ± 4.8.
[g] Field star polarimetry. South: 0.25 ± 0.05, 65. ± 5.7. Southeast: 0.31 ± 0.04, 82. ± 3.7. Southwest: 0.51 ± 0.04, 66. ± 2.2.

TABLE 3

TIME-AVERAGED WAVELENGTH-DEPENDENT POLARIZATION OBSERVATIONS[a]

Object	U	B	V	R	I	b:$PF \propto \nu^b$
0050+124	1.70 ± 0.20	1.14 ± 0.08	0.65 ± 0.06	0.36 ± 0.05	0.27 ± 0.05	+1.14
(I Zw 1)	19.8 ± 3.3	15.4 ± 2.0	17.1 ± 2.6	15.4 ± 3.9	1.6 ± 5.2	
0134+329	1.70 ± 0.20	1.92 ± 0.16	1.46 ± 0.12	1.20 ± 0.11	0.99 ± 0.12	+0.26
(3C 48)	154.2 ± 3.3	162.2 ± 2.4	163.3 ± 2.4	160.3 ± 2.8	158.9 ± 3.6	
0414−06	0.81 ± 0.16	0.86 ± 0.14	0.91 ± 0.16	1.04 ± 0.17	0.70 ± 0.39	−0.73
(3C 110)	137.3 ± 5.6	138.4 ± 4.8	148.1 ± 5.0	146.7 ± 4.7	155.9 ± 16.0	
1004+130	1.64 ± 0.17	1.13 ± 0.13	1.43 ± 0.14	0.90 ± 0.12	0.71 ± 0.15	+0.36
(4C 13.41)	57 ± 3.0	58 ± 3.3	63 ± 2.8	43 ± 3.8	24 ± 6.0	
1048−09[b]	0.79 ± 0.78	0.74 ± 0.17	...	1.47 ± 0.15	1.73 ± 0.60	−1.7
(3C 246)	105 ± 26.3	73.6 ± 6.4	...	102. ± 2.9	84.3 ± 9.9	
1114+445	2.69 ± 0.30	2.93 ± 0.25	1.99 ± 0.18	2.12 ± 0.17	2.05 ± 0.18	−0.37
	105.4 ± 3.2	100.0 ± 2.5	94.6 ± 2.7	91.3 ± 2.3	96.8 ± 2.5	
1222+228	2.56 ± 1.43	0.60 ± 0.15	...	0.82 ± 0.20	0.76 ± 0.22	−0.35
(Ton 1530)	34 ± 15.6	127.0 ± 7.0	...	147.2 ± 6.9	135.0 ± 8.2	
1254+047[b]	0.89 ± 0.34	1.22 ± 0.19	...	1.63 ± 0.26	1.98 ± 0.87	−1.8
	6 ± 10.8	170 ± 4.5	...	3 ± 4.6	12 ± 12.4	
1426+015	0.85 ± 0.11	0.84 ± 0.10	0.76 ± 0.10	...	0.51 ± 0.11	+0.27
(Mrk 1383)	84 ± 3.7	79 ± 3.4	78 ± 3.8	...	82.9 ± 6.0	
1534+580	1.46 ± 0.29	1.22 ± 0.18	0.95 ± 0.12	0.68 ± 0.11	0.52 ± 0.13	+0.51
(Mrk 290)	142.9 ± 5.7	146.7 ± 4.2	148.3 ± 3.6	147.5 ± 4.6	145.3 ± 71	
1535+547	3.77 ± 0.22	3.19 ± 0.19	2.60 ± 0.14	2.10 ± 0.11	2.29 ± 0.12	−0.57
(Mrk 486)	142.0 ± 1.7	138.4 ± 1.7	142.7 ± 1.6	138.8 ± 1.5	143.2 ± 1.6	
1552+08	3.07 ± 0.58	1.96 ± 0.18	...	1.32 ± 0.18	1.31 ± 0.31	+0.20
	69 ± 5.4	88 ± 2.6	...	76 ± 3.9	78 ± 6.7	
2209+185	...	0.90 ± 0.37	0.34 ± 0.18	0.35 ± 0.14	0.32 ± 0.15	+0.58
	...	12.6 ± 11.7	3.7 ± 14.4	4.7 ± 11.3	42.1 ± 13.4	

[a] Polarization (%)/Position Angle (degree).
[b] UV and optical continuum mismatch, no continuum fits.

reddening from dust in the Milky Way, assuming a standard $E_{(B-V)_{mw}}$/H I ratio (Burstein & Heiles 1978), and normal reddening law. The corrections were quite small since most of the objects are at high Galactic latitude. Corrections for *internal* reddenings are also likely to be minor. The great majority of them were selected by their ultraviolet excesses, either in the PG or Markarian surveys. The extremely small absorption of soft X-rays in Mrk 509, NGC 5548, and 3C 273 require very small $E(B-V)_{\rm int} < 0.05$, 0.1, and 0.05, respectively, for standard dust/gas ratios (Turner & Pounds 1989).

3.2. *Continuum Fits and Component Fluxes*

To fit the various spectral components in the multi-wavelength continuum, we used the methods of Malkan & Sargent (1982) and Malkan (1983). The long-wavelength continuum was first fitted with a power law of slope α. The power law is a negligible component at optical wavelengths for several of the quasars in our program, including 1004+130 (4C 13.41), 1151+117, and 1552+08. The deconvolution of optical continua for these objects should be valid regardless of the physical reality of the power-law component. For most of the program objects, the flux in our broad-band filters was dominated by the continuum. The principal exception was the R filter, where, for several low-redshift AGNs, the equivalent width of Hα indicates that this line produced up to 20% of the total flux. These cases are indicated in Table 5. The estimated flux for the pseudocontinuum of Fe II line and Balmer continuum emission was included, as in Edelson & Malkan (1986). The remaining ultraviolet excess continuum was fitted with a two-parameter model of a relativistic, optically thick, geometrically thin accretion disk (Sun & Malkan 1989). In the most luminous quasars, the flux contribution from starlight was less than 10%. In less luminous objects, we adopted the stellar flux estimates of Neugebauer et al. (1987) or used unpublished direct images. Even though these estimates could be in error by as much as 25%, this would generally have led to only small errors in our determination of the nonstellar continuum compared with the much weaker starlight. The exceptions were the Seyfert 1 galaxies and PG 2209+185, which appears to reside in a luminous elliptical galaxy (Neugebauer, et al. 1985). Underestimating the starlight in these objects would have biased us in favor of hypotheses which predict strong increases of polarization in the blue. We discuss several polarization hypotheses in the next section, including thermal and dust-scattering models which would be affected by an overestimation of polarization at higher frequencies.

The model parameters for the power-law flux, Balmer continuum flux, black hole mass, and accretion rate, which best fit the observed continua are summarized in Table 4. Had we assumed a thermal origin for the near-infrared flux, the black hole masses would have to be doubled and the accretion rates increased about 10% (Malkan 1989).

Table 5 lists the proportions of power law, starlight, Balmer continuum, and thermal emission contributing to the total flux in each of the UBVRI bands. The continuum fits were also extrapolated to a mid-ultraviolet band "MU" centered on 2100 Å, and a far-ultraviolet "FU" band centered on 1300 Å, as well as the J (1.25 μm), K (2.2 μm), and L (3.8 μm) near-IR bands.

3.3. *Uncertainties in Continuum Fits*

When an individual continuum component dominated a spectral region, its flux contribution could be determined accurately (to within 10%). Since the assumed "power-law" component always dominated the infrared fluxes, its slope was well

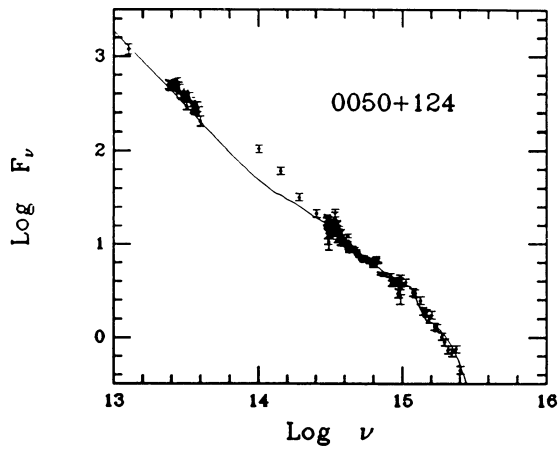

FIG. 1*a*

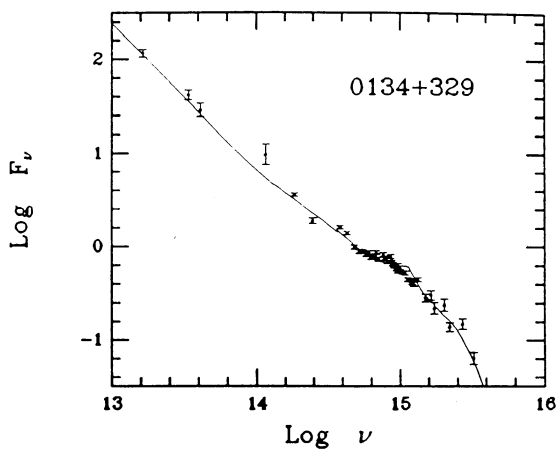

FIG. 1*b*

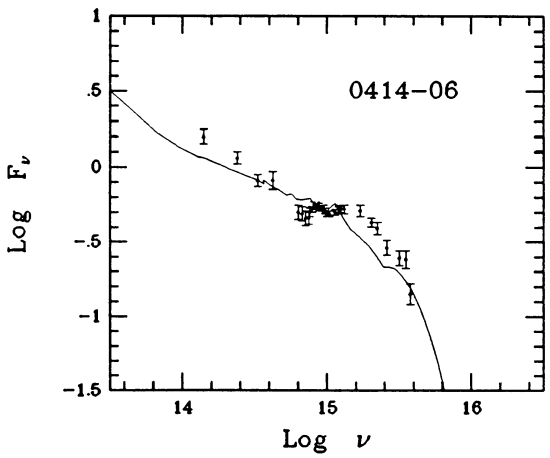

FIG. 1*c*

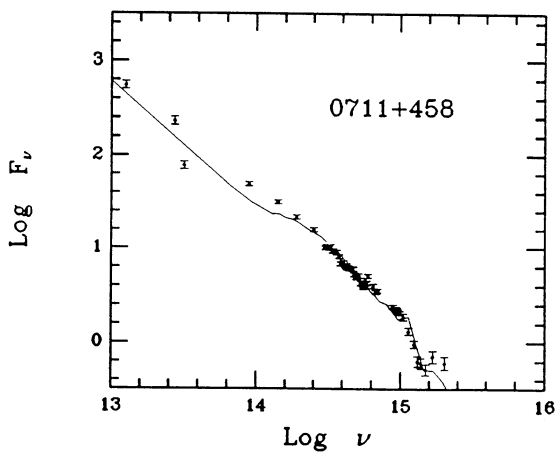

FIG. 1*d*

FIG. 1.—Spectral energy distributions for the program quasars and Seyfert 1 galaxies. Data points are shown with error bars. Best multicomponent fit is shown as a solid line.

determined, with an accuracy of ± 0.2. The uncertainties in the starlight component were negligible for the majority of the AGNs. The recombination and thermal model parameters in the multicomponent fits were varied within the limits allowed by the data, and the uncertainties estimated in these continuum components for each of the wavebands. We defer further discussion of the uncertainties in continuum fits until the results of the polarization modeling have been presented.

The multiwavelength continuum fits were based on observations which were usually not contemporaneous with the polarimetry. Fortunately, repeated flux measurements have shown that most of the normal quasars and Seyfert galaxies in this sample exhibit only small-amplitude flux variability (less than 0.4 mag) at optical wavelengths (Allan & Keel 1993). The only two exceptions, PG 1048−09 and PG 1254+047, are discussed below. More critically, the *shape* of the optical continuum did not change substantially (Cutri et al. 1985). Finally, our data published here do not indicate that the polarizations vary significantly with time (as is discussed further below). Therefore, we believe that the nonsimultaneity of our photometry and polarimetry is not a significant source of uncertainty in our procedure.

We argued in the previous section that there was little evidence that these spectra required significant corrections for internal reddening. Even if they were dereddened, to first order, our component-fitting results would be affected very little. This is because our polarization model predictions which we tested depend upon *observed* components as distinct from the *dereddened* components. Our estimates of the relative contributions of each component to the U, B, V, R, and I fluxes would still be approximately correct, because reddening would have a roughly similar effect on all components (i.e., making all of them fainter and redder).

4. POLARIZATION MODEL FITTING OF THE DATA

4.1. *Polarization Models and Limitations*

Each of the several polarization mechanisms that have been proposed for AGNs, predicts a different wavelength dependence of polarization. We describe these polarization hypotheses and our models, and then compare model predictions with observations.

(1) *Power Law Hypotheses (PL).*—An apparent power-law flux component gives rise to the observed polarization, prob-

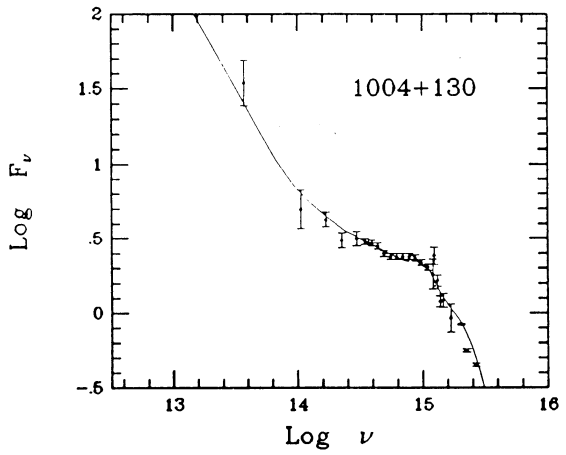

FIG. 1*e*

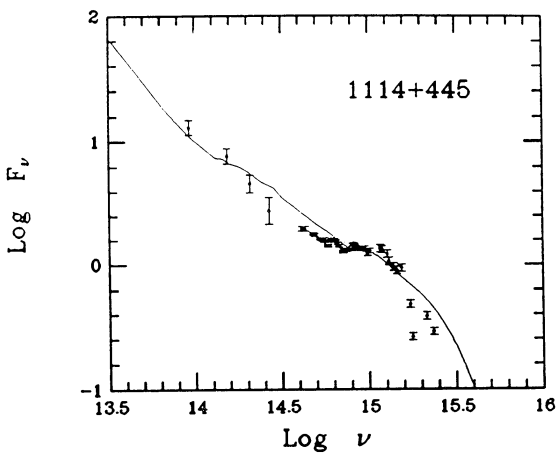

FIG. 1*f*

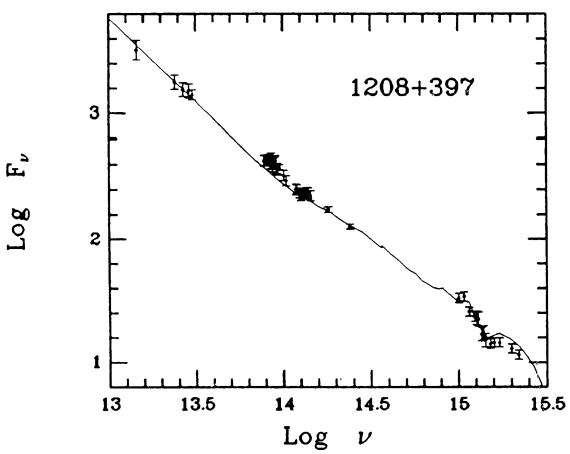

FIG. 1*g*

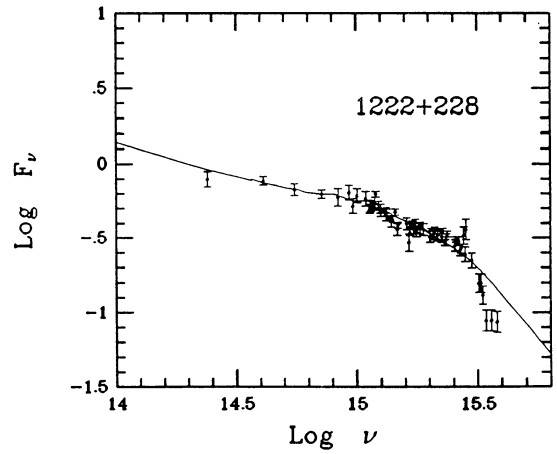

FIG. 1*h*

ably due to synchrotron emission. If this component is presumed to have wavelength-independent polarization, the observed polarized flux will be proportional to the power-law flux at each wavelength. There is one constant of proportionality—the percentage of polarization of the power law. Since the power-law flux has a negative slope when plotted against increasing frequency, this hypothesis predicts that the total polarized flux observed from the object should *decrease* with increasing frequency.

Several dust scattering hypotheses (nos. 2, 3, 4) assume that all of the nuclear light, including broad line region (BLR) emission, passes through a nonspherical distribution of dust grains,

TABLE 4

COMPONENT FITTING PARAMETERS

Object	α_{pl}	F_{pl} @ 5400 Å (mJy)	F_b 3646 Å (mJy)	BH Mass ($M_\odot$)	Accretion Rate ($M_\odot$ yr^{-1})
0050+124	−1.65	2.50	0.80	7.0E+08	0.05
0134+329	−1.60	0.40	0.30	1.0E+09	0.26
0414−06	−0.90	0.22	0.01	9.0E+08	2.50
0711+458[a]	−1.40	2.20	1.00	3.0E+08	0.02
1004+130	−1.55	0.35	0.50	1.5E+09	0.50
1114+445	−1.80	0.37	0.30	8.0E+08	0.06
1208+397[a]	−1.37	24.0	10.0	1.2E+07	0.0025
1222+228	−0.80	0.30	0.04	5.3E+09	19.0
1415+253[a]	−1.40	5.00	2.50	9.0E+07	0.006
1426+015	−1.15	2.80	4.00	3.0E+08	0.15
1534+580	−1.50	1.00	1.10	4.0E+07	0.019
1535+547	−1.30	1.60	1.40	1.1E+09	0.006
1552+08	−1.40	0.16	0.50	1.5E+09	0.048
2041−109[a]	−1.25	5.50	8.00	7.0E+07	0.075
2209+185	−1.40	0.30	1.40	9.0E+08	0.03

[a] Objects for which we have continuum fits and polarimetry has already been published.

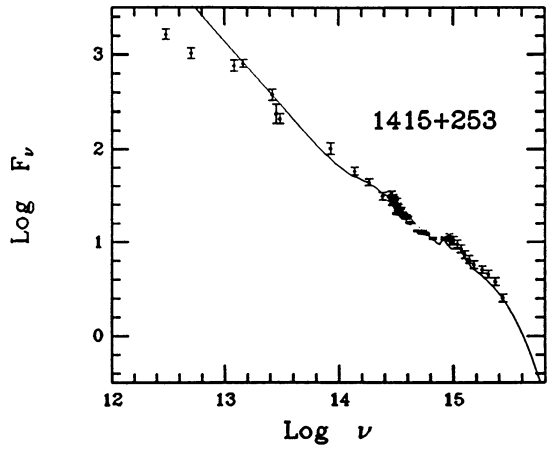

FIG. 1*i*

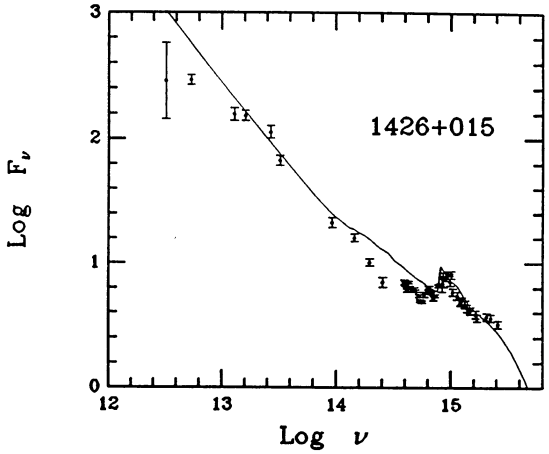

FIG. 1*j*

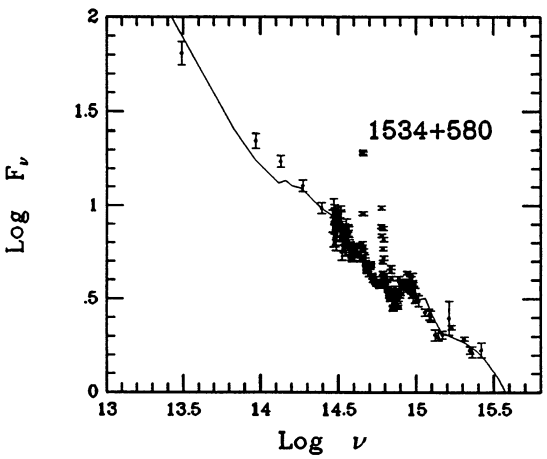

FIG. 1*k*

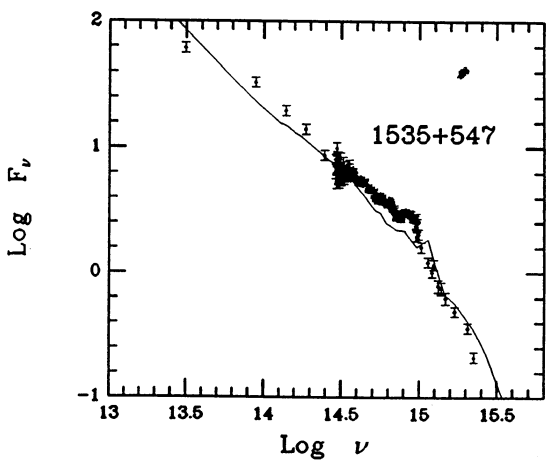

FIG. 1*l*

which scatter a wavelength-dependent fraction of the light. The observed polarized flux is proportional to the product of the original nuclear flux, the fraction of the flux which is scattered, and the polarizing efficiency of the dust. These three factors can be different functions of wavelength in our different dust models. Since the nonstellar or nuclear light is 80%–95% of the total light in most of these objects, the dust hypotheses predict that the polarized flux will be roughly proportional to the total observed spectrum of the object, potentially modified by the peak polarizing efficiency of the grains, and by the dust-scattering cross section. These assumptions are not tied to particular geometrical distributions of the dust; special configurations, such as dust arranged in a "warped disk," are not excluded.

(2) *MRN Hypothesis.*—Using the dust grain distribution of Mathis, Rumpl, & Nordsieck (1977, hereafter MRN). White (1979) calculated the scattering cross section and the expected minimum linear polarization, as a function of wavelength. We used this to estimate the P2 matrix element as the peak polarization times the scattering cross section. Fortunately, for a standard dust mixture, geometrical considerations are not overwhelmingly important at visual and near-ultraviolet wavelengths. The calculations of White (1979), show that the mean value of the cosine of the scattering angle (the asymmetry parameter g) varies by approximately 15% from 2000 to 6000 Å. In Figure 2, we show the P2 matrix element (relative polarized flux per unit nuclear continuum) calculated using White's formulae and figures, as a function of wavelength and scattering angle. It shows that our simple approximation in the MRN hypothesis matches well the wavelength dependence for angles of 30°–90°. Although it somewhat overestimates the polarized flux from dust at 120° and 150° (i.e., behind the central source), such backscattering is probably not very important. Because of the extreme forward-scattering of the interstellar dust, most of the observed polarization would arise from dust to the side or front of the continuum emitter (at angles of 30°–90° degrees). Our MRN extrapolation to wavelengths longer than 1 μm is more uncertain.

(3) λ^{-1} *Hypothesis.*—The nonstellar continuum is polarized by a nonspherical distribution of grains which produce polarization inversely proportional to wavelength (i.e., $P2 \propto \lambda^{-1}$). Here we are assuming polarization caused by scattering; Martin et al. (1982) argued that *transmission* of nuclear continuum light through very small dust grains could explain the strong rise of polarization with frequency in the luminous Seyfert 1 galaxy IC 4329A. Our model receives some motivation from the fact that polarization proportional to λ^{-1} is also observed in some dusty *IRAS*-selected quasars, such as IRAS 13349+2438 (Wills et al.1989).

(4) λ^{-2} *Hypothesis.*—Another variant of the dust-scattering

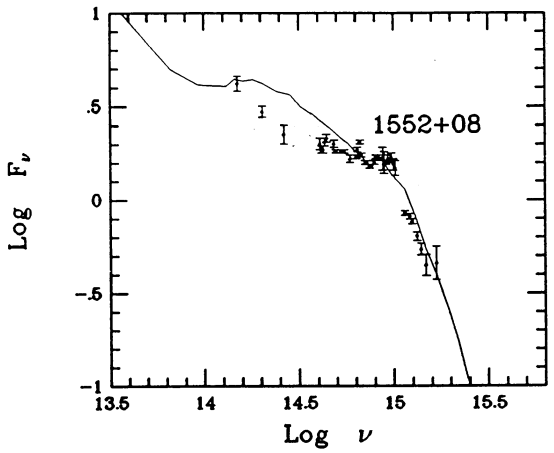

FIG. 1*m*

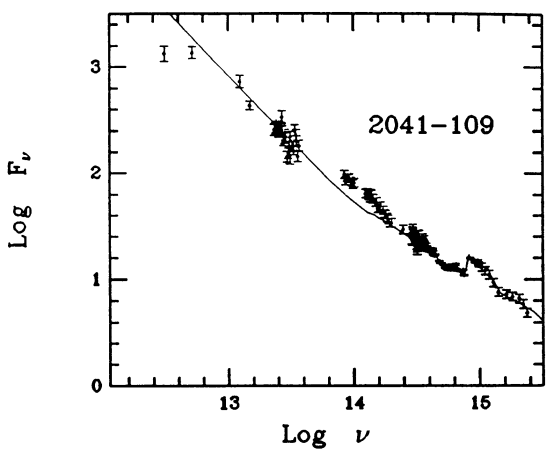

FIG. 1*n*

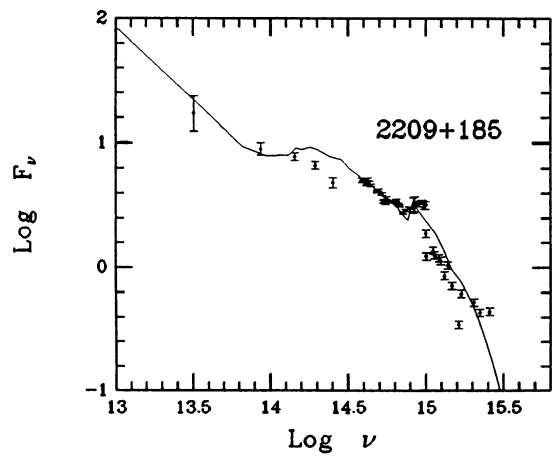

FIG. 1*o*

model is that the nonstellar continuum is polarized proportional to λ^{-2}. This stronger wavelength dependence of polarization has been seen in a few very dusty *IRAS* quasars, such as IRAS 14026+4341 (Wills et al. 1989), and appears to be the strongest wavelength dependence that any realistic population of dust grains is likely to produce. Higher proportionalities (up to λ^{-4}) are *theoretically* possible in the Rayleigh limit of infinitesimally small grains.

(5) *Nonstellar Continuum Hypothesis* (*Ns*).—The polarized flux arises from scattering by a nonspherical distribution of particles surrounding the nucleus, and is proportional to the total flux from the object minus the starlight, or alternately, minus the starlight and the Balmer recombination emission from the BLR. Specifically, this hypothesized wavelength-dependent polarization of the nuclear continuum could be interpreted as due to scattering by a nonspherical distribution of free electrons (Antonucci 1988). The Ns hypothesis is simply another variant of scattering hypotheses nos. 2–4, except that the polarization is independent of wavelength.

(6) *Thermal Component Hypothesis* (*Th*).—The polarization originates in the blue/ultraviolet excess component, which has a constant percentage of polarization at all wavelengths. If we attribute the infrared emission to thermally emitting dust grains rather than a nonthermal power law (see below), this component would dominate the UV and optical flux from most of the quasars. In this case the only true nuclear continuum component would be the blue/UV thermal component, and hypotheses 5 and 6 would become indistinguishable.

(7) *Interstellar Transmission Hypothesis* (*IT*).—Light from the nucleus is scattered by interstellar dust in the galaxy in which the AGN is embedded. This is expected when, for example, the galaxy is viewed edge-on. From observations in our own Galaxy the polarization of transmitted light obeys a simple empirical formula:

$$P(\lambda) = P_{\max} \exp\left[-1.15 \ln^2(\lambda_{\max}/\lambda)\right],$$

where $\lambda_{\max}$ is usually around 5500 Å (Serkowski, Mathewson, & Ford 1975).

Combinations of these seven different polarizing mechanisms within a single object are possible. However, combinations are not the simplest explanation, and the near constancy of the polarization position angle across the spectrum suggests that the polarization is likely due to a single mechanism. A more complicated interpretation would be that more than one mechanism is operating, but that they share a common symmetry axis.

Several of these hypotheses appear to be ruled out easily by the observed wavelength dependence of polarization. For example, if polarization measurements with broad red and blue filters established that the polarization rises with frequency,

TABLE 5

COMPONENT FLUXES[a]

AGN	Component	FU	MU	*U*	*B*	*V*	*R*	*I*	*J*	*K*	*L*
0050+124 (I Zw 1)	Stars	0.02	0.01	0.02	0.08	0.15	0.20	0.24	0.29	0.18	0.06
	Power	0.14	0.12	0.16	0.20	0.24	0.28	0.32	0.43	0.66	0.86
	Thermal	0.84	0.78	0.65	0.61	0.53	0.46	0.37	0.24	0.13	0.07
	Recomb	<0.01	0.08	0.16	0.10	0.08	0.06	0.07	0.04	0.02	0.02
0134+329 (3C 48)	Stars	0.01	<0.01	<0.01	0.01	0.03	0.09	0.12	0.17	0.16	0.01
	Power	0.19	0.17	0.15	0.20	0.29	0.36	0.41	0.52	0.69	0.86
	Thermal	0.80	0.80	0.48	0.46	0.52	0.48	0.40	0.24	0.12	0.01
	Recomb	<0.01	0.03	0.37	0.33	0.16	0.07	0.07	0.06	0.03	0.02
0414−06 (3C 110)[b]	Power	0.16	0.16	0.18	0.17	0.22	0.24	0.29	0.36	0.49	0.61
	Thermal	0.84	0.84	0.76	0.57	0.65	0.60	0.58	0.46	0.32	0.22
	Recomb	<0.01	<0.01	0.06	0.26	0.12	0.16	0.11	0.13	0.10	0.09
0711+458 (Mrk 376)	Stars	0.04	0.03	0.05	0.16	0.26	0.33	0.37	0.43	0.29	0.11
	Power	0.26	0.22	0.23	0.27	0.29	0.31	0.32	0.39	0.58	0.81
	Thermal	0.69	0.57	0.38	0.34	0.27	0.23	0.17	0.11	0.07	0.04
	Recomb	<0.01	0.18	0.34	0.23	0.18	0.13	0.14	0.07	0.06	0.04
1004+130 (4C 13.41)[b]	Power	0.04	0.04	0.05	0.06	0.10	0.12	0.16	0.27	0.48	0.70
	Thermal	0.96	0.94	0.79	0.74	0.85	0.82	0.77	0.64	0.44	0.26
	Recomb	<0.01	0.02	0.16	0.20	0.04	0.04	0.04	0.03	0.03	0.02
1114+445	Stars	0.02	0.01	0.02	0.07	0.20	0.28	0.35	0.46	0.33	0.12
	Power	0.06	0.07	0.10	0.14	0.17	0.19	0.23	0.30	0.53	0.80
	Thermal	0.92	0.89	0.74	0.76	0.62	0.52	0.41	0.24	0.14	0.07
	Recomb	<0.01	0.03	0.15	0.03	0.01	0.01	0.01	<0.01	<0.01	<0.01
1208+397 (NGC 4151)	Stars	<0.01	0.01	0.03	0.12	0.16	0.19	0.22	0.25	0.13	0.05
	Power	0.13	0.18	0.25	0.34	0.38	0.42	0.45	0.57	0.79	0.91
	Thermal	0.86	0.68	0.45	0.42	0.35	0.28	0.21	0.12	0.04	0.01
	Recomb	<0.01	0.13	0.27	0.12	0.11	0.11	0.12	0.06	0.04	0.03
1222+228 (Ton 1530)[b]	Power	0.81	0.48	0.32	0.31	0.30	0.30	0.30	0.38	0.50	0.61
	Thermal	0.19	0.52	0.68	0.69	0.68	0.65	0.58	0.57	0.45	0.36
	Recomb	<0.01	<0.01	<0.01	<0.01	0.02	0.05	0.12	0.06	0.04	0.03
1415+253 (NGC 5548)	Stars	0.01	0.01	0.03	0.15	0.22	0.28	0.33	0.38	0.22	0.08
	Power	0.18	0.21	0.25	0.33	0.36	0.38	0.39	0.46	0.68	0.87
	Thermal	0.80	0.67	0.45	0.44	0.35	0.28	0.21	0.13	0.07	0.03
	Recomb	<0.01	0.11	0.27	0.08	0.07	0.06	0.07	0.03	0.02	0.02
1426+015 (Mrk 1383)	Stars	<0.01	<0.01	<0.01	0.03	0.08	0.11	0.15	0.22	0.16	0.06
	Power	0.16	0.18	0.19	0.33	0.37	0.41	0.44	0.52	0.68	0.85
	Thermal	0.83	0.71	0.44	0.59	0.52	0.45	0.37	0.24	0.14	0.07
	Recomb	<0.01	0.10	0.37	0.05	0.04	0.03	0.04	0.02	0.02	0.01
1534+580 (Mrk 290)[c]	Stars	<0.01	<0.01	0.03	0.14	0.23	0.31	0.38	0.47	0.32	0.13
	Power	0.05	0.08	0.12	0.19	0.22	0.24	0.26	0.34	0.57	0.82
	Thermal	0.94	0.82	0.55	0.57	0.46	0.38	0.28	0.16	0.07	0.03
	Recomb	<0.01	0.09	0.30	0.10	0.09	0.07	0.08	0.04	0.03	0.02
1535+547 (Mrk 486)	Stars	0.02	0.01	0.02	0.09	0.14	0.18	0.20	0.24	0.14	0.05
	Power	0.48	0.41	0.40	0.49	0.51	0.54	0.54	0.62	0.78	0.90
	Thermal	0.49	0.37	0.23	0.21	0.17	0.14	0.10	0.06	0.03	0.02
	Recomb	0.01	0.21	0.35	0.21	0.18	0.14	0.15	0.07	0.05	0.03
1552+08	Stars	0.03	0.01	0.01	0.05	0.13	0.19	0.25	0.39	0.37	0.20
	Power	0.15	0.06	0.05	0.06	0.07	0.08	0.09	0.12	0.22	0.43
	Thermal	0.80	0.82	0.70	0.82	0.77	0.71	0.63	0.47	0.39	0.34
	Recomb	0.02	0.11	0.24	0.07	0.03	0.03	0.04	0.02	0.02	0.02
2041−109 (Mrk 509)	Stars	<0.01	<0.01	<0.01	0.05	0.09	0.13	0.17	0.23	0.15	0.05
	Power	0.13	0.16	0.17	0.32	0.36	0.41	0.44	0.54	0.74	0.88
	Thermal	0.86	0.67	0.36	0.48	0.40	0.35	0.26	0.15	0.06	0.02
	Recomb	<0.01	0.16	0.45	0.15	0.14	0.11	0.13	0.07	0.05	0.04
2209+185	Stars	0.03	0.01	0.02	0.11	0.22	0.29	0.38	0.52	0.48	0.28
	Power	0.09	0.05	0.04	0.07	0.07	0.08	0.09	0.11	0.21	0.44
	Thermal	0.85	0.82	0.62	0.80	0.70	0.62	0.52	0.36	0.30	0.27
	Recomb	0.03	0.12	0.32	0.02	0.01	0.01	0.01	<0.01	<0.01	<0.01

[a] Fraction of total flux.
[b] Stars contribute less than 0.10 of the total flux in all bands.
[c] Hα produces more than 20% of the flux in the R band.

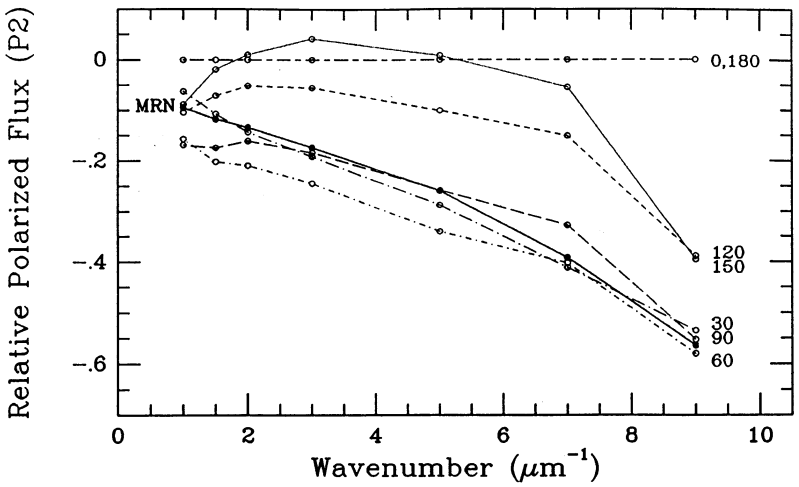

FIG. 2.—Relative polarization (i.e., the P2 matrix element) vs. wavenumber, for the MRN hypothesis described in this paper, compared with specific scattering angles (with calculations from White 1979).

this would be sufficient to eliminate the power-law (PL) hypothesis, since that component's polarized flux should be increasing at longer wavelengths. However, the differences between other hypotheses are more subtle: several dust-scattering models, as well as the thermal hypothesis, predict a general rise of polarization with frequency, as observed by SMA. A choice between the models cannot be made simply from blue and red polarimetry alone; the multicomponent nature of the continuum requires more detailed observations and analysis. For example, Laor, Netzer, & Piran (1990) apply the thermal hypothesis to the SMA data in Figure 7 of their paper, but only as a consistency test. The observations might be explained equally well with several of the dust-scattering hypotheses described above. In this paper we show how multi-wavelength polarimetry and modeling can be used to further differentiate between the competing hypotheses.

4.2. *Polarization Model Fitting*

We have compared the observed wavelength dependence of polarization with predictions of seven hypotheses proposed to explain its origins. These hypotheses are polarization originating from (1) the long-wavelength "power law," (2)–(4) scattering by dust grains in the neighborhood of the nucleus with properties described by MRN, with $P \propto \lambda^{-1}$ (Martin et al. 1982), and with $P \propto \lambda^{-2}$, (5) all the nonstellar light, (6) the blue thermal component, and (7) transmission through aligned dust grains in the host galaxy (Serkowski et al. 1975). These seven models are represented by the line types shown in Figure 3*a*.

Deciding how well a given hypothesis fits the polarimetric data requires some model-dependent interpretation. Testing these models requires separating the nonstellar continuum flux from the starlight of the underlying galaxy (which is presumed to be unpolarized). Some variants of these models also require estimating the flux emitted by the BLR (particularly the Balmer continuum and Fe II pseudo-continuum of blended emission lines), to separate it from the nuclear flux generated in the more compact central engine. Two of the hypotheses depend upon estimates of the flux from individual continuum components: a "power-law" and a thermal component. Hence, the testing of these last two hypotheses is the most model-dependent.

We fit simple models of these polarization mechanisms to the data, solving for any constants of proportionality by the method of least-squares. Fits to individual data points were weighted inversely proportional to the square of the standard deviations of the polarized flux measurements. The results are displayed in Figures 3*b*–3*p* which give the polarized fluxes at the measured *UBVRI* data points (with error bars), and multiple model fits indicated by the line types of Figure 3*a*. We calculate the χ^2 errors resulting from the application of each polarization model to the data for each object. The χ^2 errors have been normalized by their number of degrees of freedom (i.e., divided by the number of polarization measurements minus one). For some of our objects the preferred model fit has a χ^2 of only a few and is significantly smaller than that of rival models. Often there are two or more models which due to the uncertainties of the modeling cannot be distinguished. In each case, several of the models appear decisively ruled out.

We evaluated the errors in the polarization model-fitting process by modifying the multiwavelength fit parameters within the uncertainties of the flux measurements. We then refit the polarization data for the objects using a range of values for the continuum components. For almost all the program objects, the χ^2 changed very little (typically by less than 10%). In a few cases, however, the revised fits did produce changes in values of χ^2 sufficient to change the ranking of the best two polarization hypotheses.

4.3. *Polarization Model Fits: The Template Objects*

Before applying our polarization models to the program AGNs, we tested our methodology on some objects for which the origin of the polarization is believed to be understood. These template objects included known OVV blazars (AO 0235+164, OJ 287, and B2 1156+295), and a dusty AGN (Mrk 486).

For the blazars, we had published *UBVRIJK* polarimetry (Smith et al. 1987), but no multiwavelength continuum data. We therefore assumed a single power-law component dominated the continuum and was the source of polarized flux from either synchrotron emision or dust scattering, obviating the need for a multicomponent continuum fit. In this special case, the nonstellar and power-law models are the same, and the

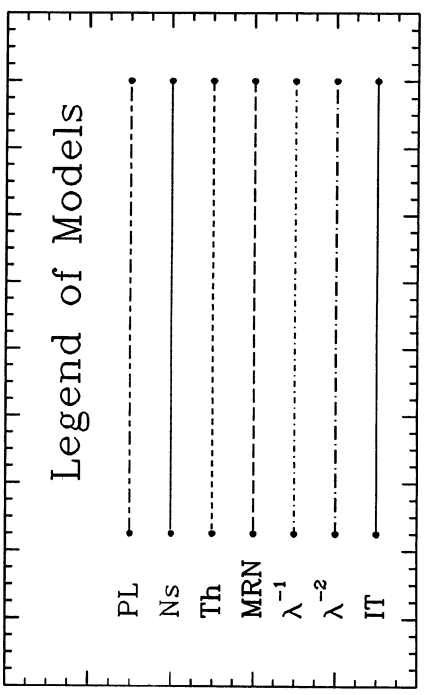

FIG. 3a

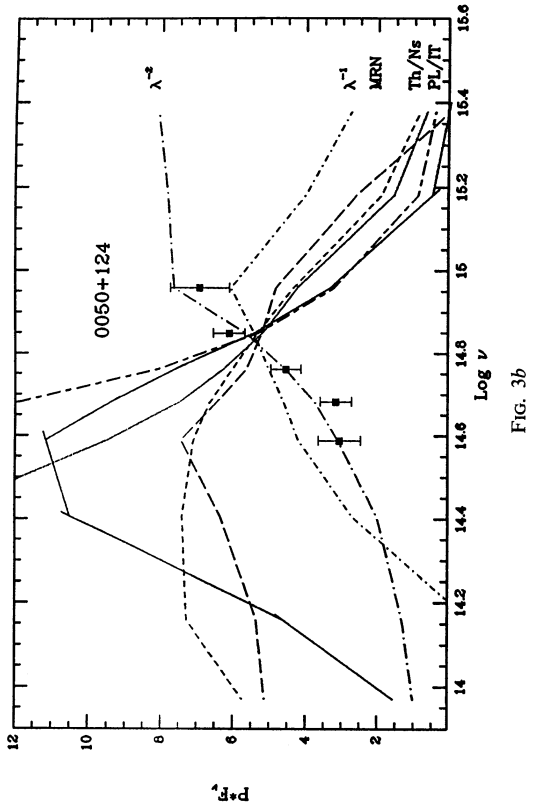

FIG. 3b

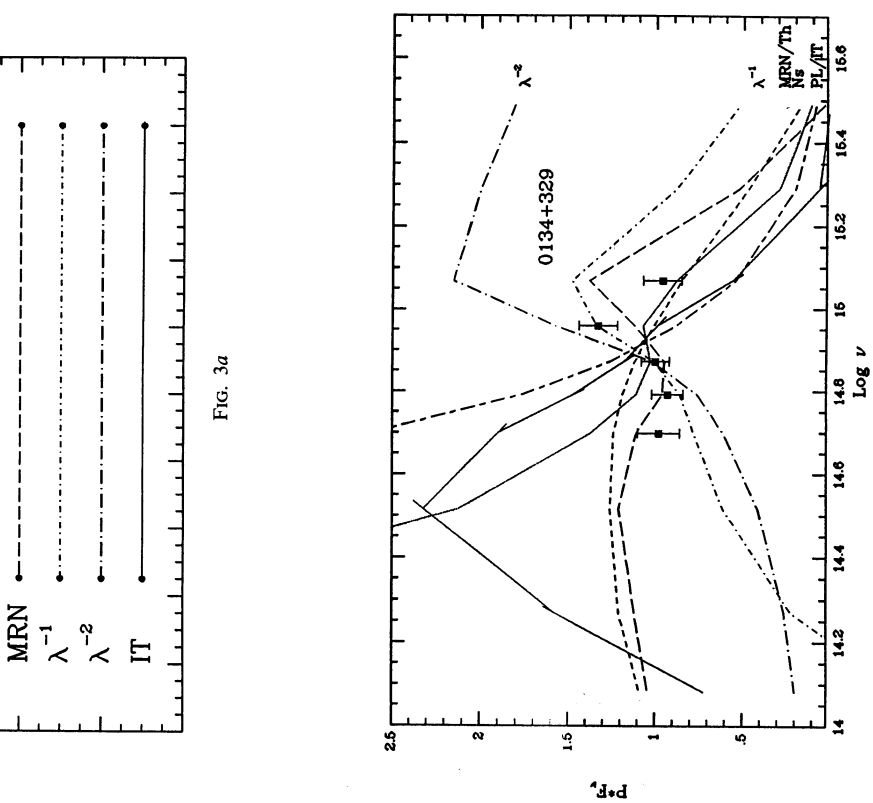

FIG. 3c

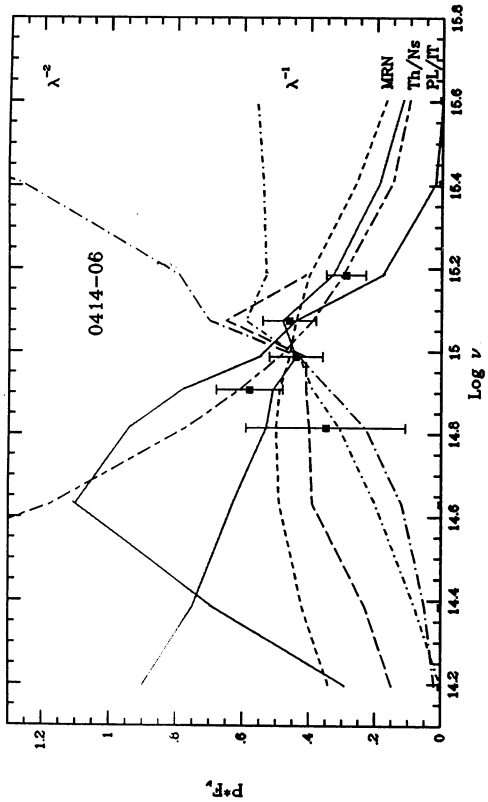

FIG. 3d

FIG. 3.—(*a*) Legend of polarization models indicating line type. (*b*)–(*p*) Polarized fluxes for program quasars and Seyfert 1 galaxies. *UBVRI* data points are shown with error bars. Models are shown with line types as indicated in Fig. 3*a*.

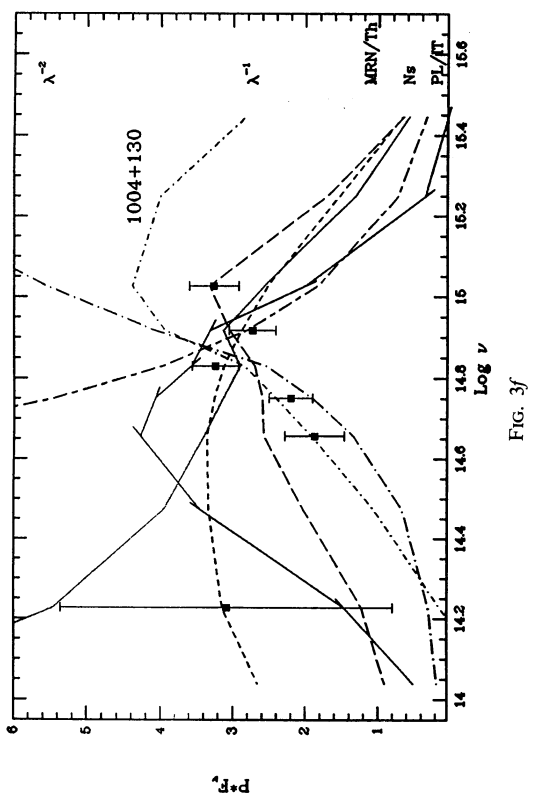

FIG. 3f

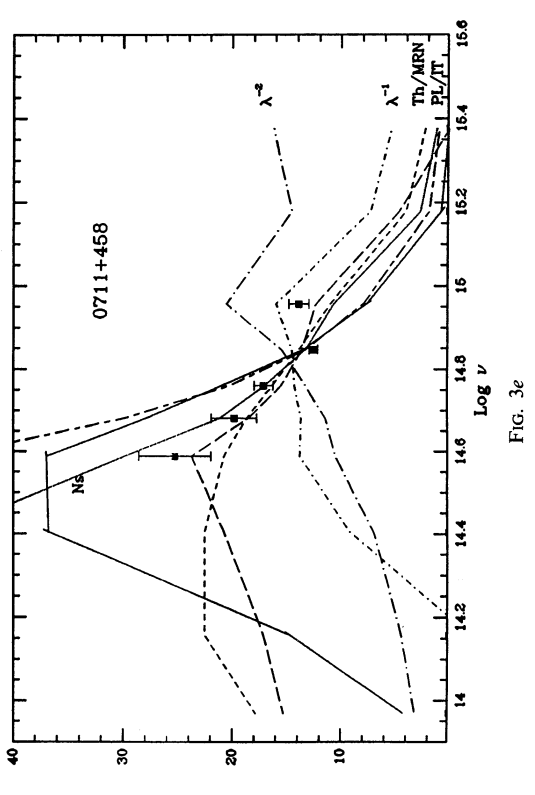

FIG. 3e

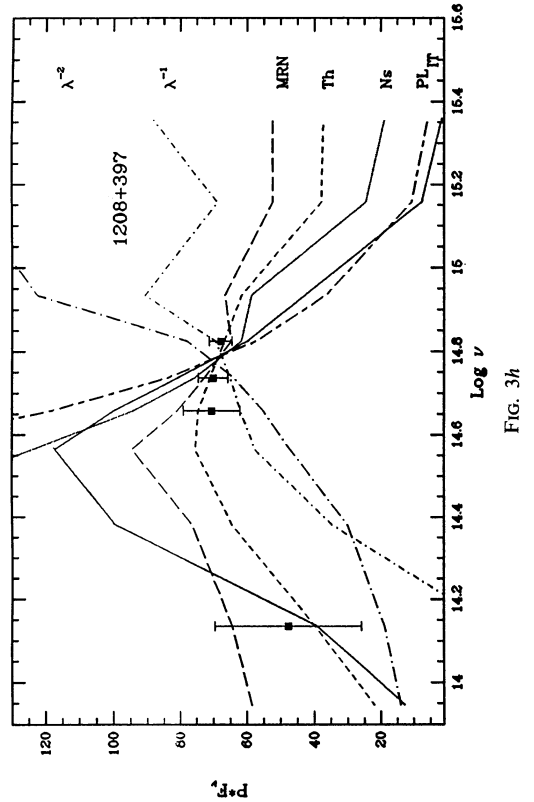

FIG. 3h

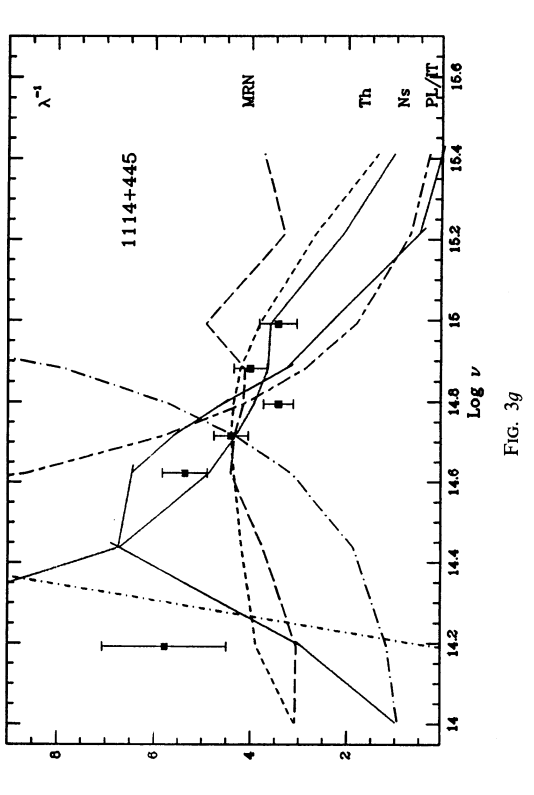

FIG. 3g

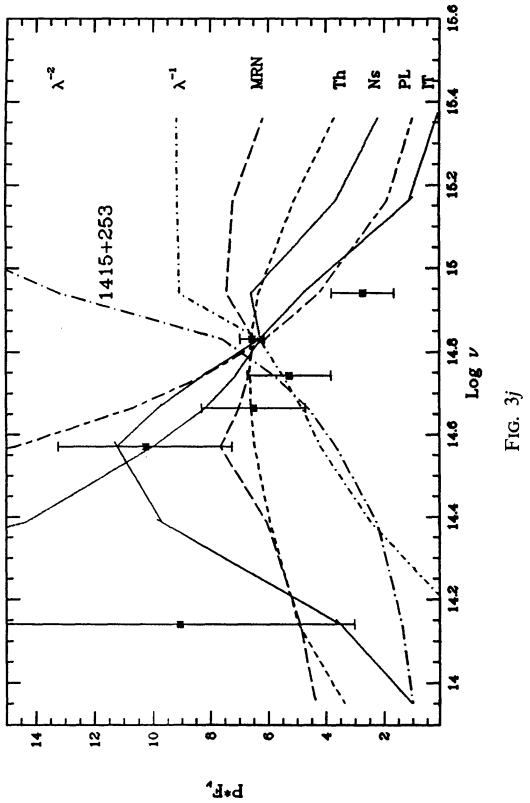

FIG. 3j

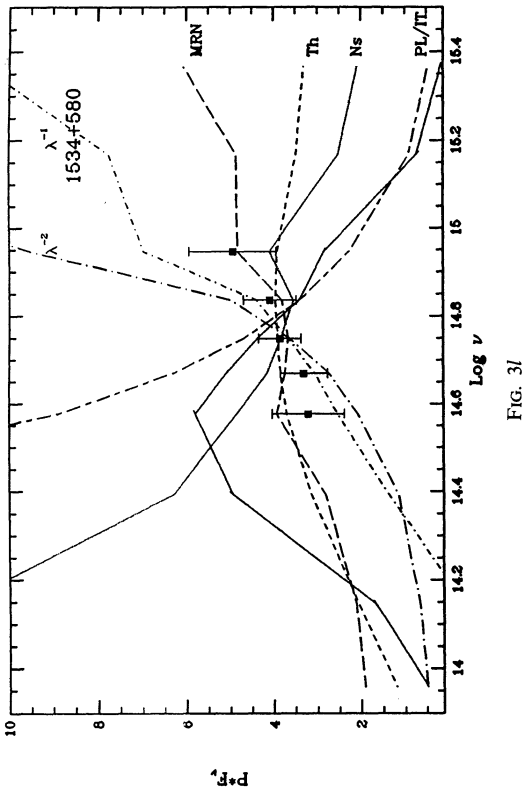

FIG. 3l

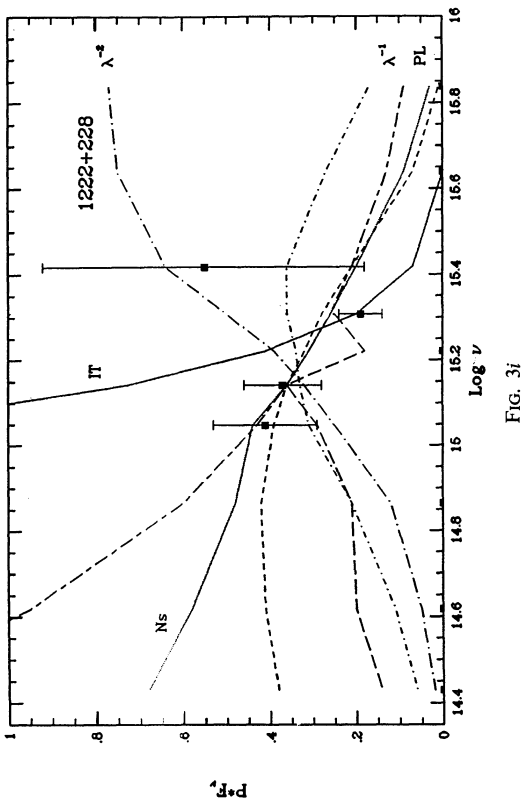

FIG. 3i

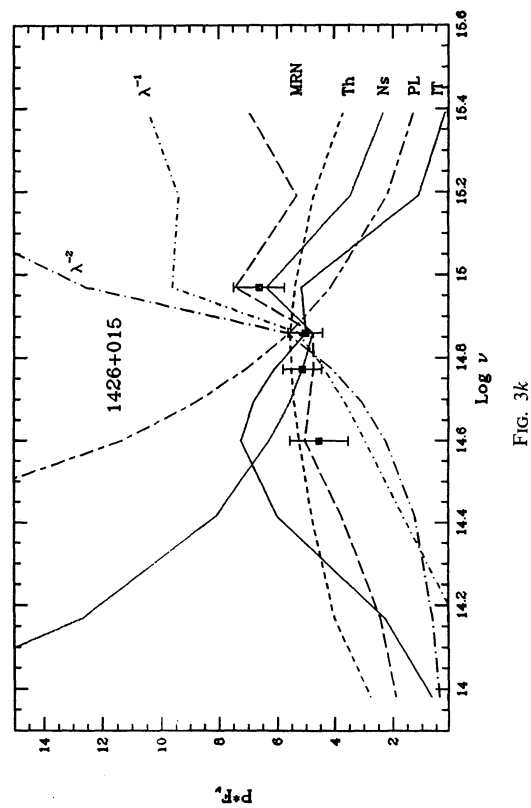

FIG. 3k

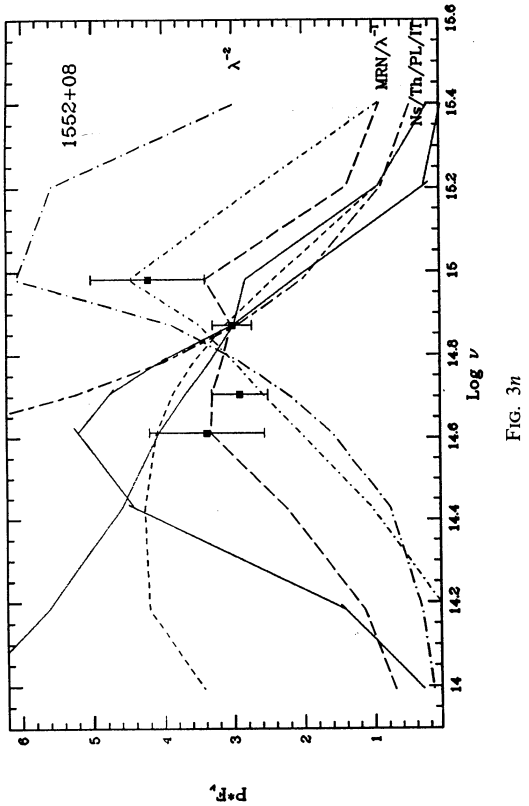

FIG. 3n

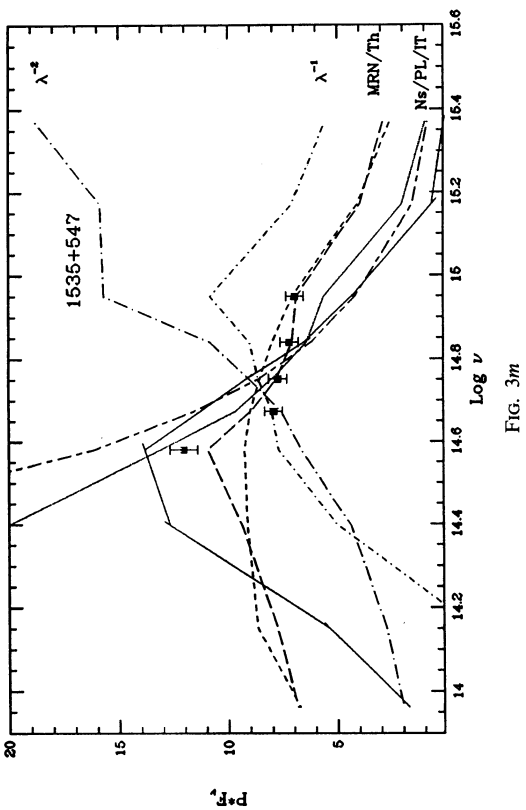

FIG. 3m

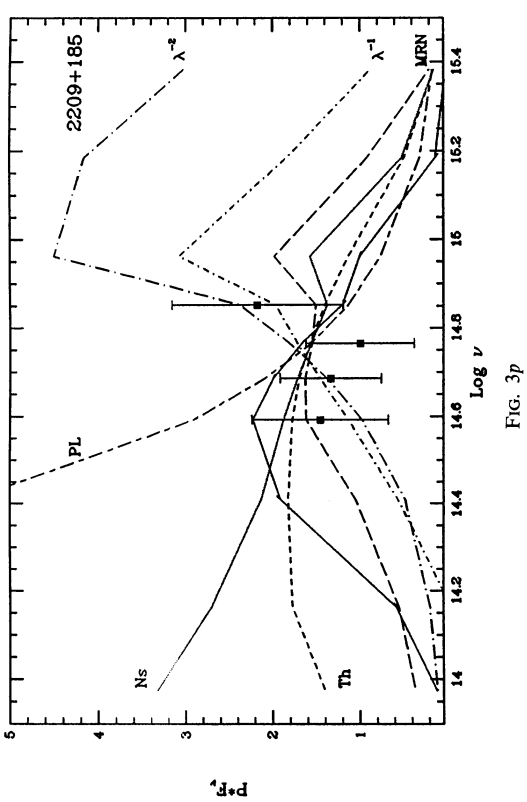

FIG. 3p

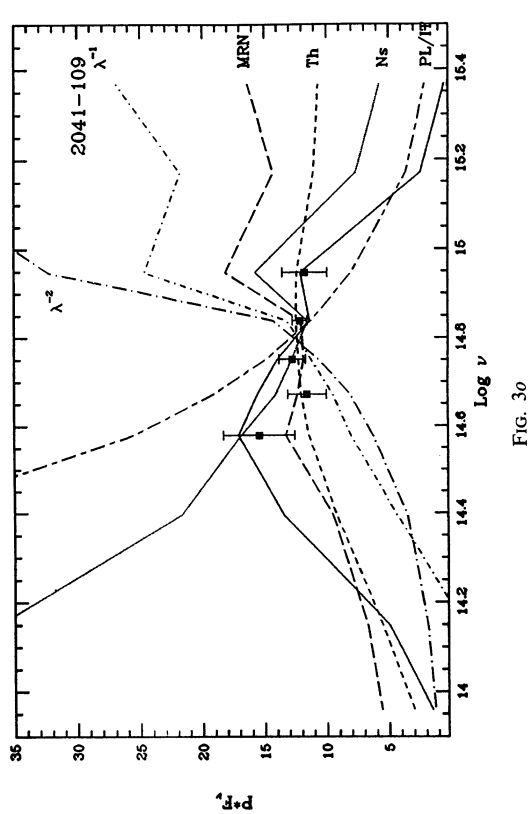

FIG. 3o

TABLE 6

POLARIZATION HYPOTHESES

Object	Power Law	Nonstellar	Thermal	MRN	λ^{-1}	λ^{-2}	IT
AO 0235+164	**5.96**[b]	...	...	15.1	82.3	130.0	...
OJ 287	**8.84**[b]	...	...	482.	2113.	2754.	...
B2 1156+295	**57.1**[b]	...	...	306.	1690.	3200.	...
1535+547 (Mrk 486)	43.5	8.7	8.3	**2.3**	39.8	154.5	32.0
0050+124 (I Zw 1)	289.	61.8	33.8	32.3	4.93	**0.95**	116.
0134+329 (3C 48)	79.3	**5.15**	6.25	**4.70**	6.15	32.5	31.0
0414−06 (3C 110)	1.09	**0.42**	1.22	3.52	5.85	21.6	3.98
0711+458 (Mrk 376)	29.8	**4.50**	6.00	**3.50**	15.2	40.0	49.4
1004+130 (4C 13.41)	122.	6.34	6.14	**1.84**	5.90	14.7	18.6
1114+445	274.	7.36	**3.36**	**5.74**	...	161.	9.58
1208+397 (NGC 4151)	393.	71.3	**0.17**	1.10	3.53	5.23	7.87
1222+228 (Ton 1530)	**0.85**	**0.87**	1.23	...	4.00	12.8	24.2
1415+253 (NGC 5548)	17.2	5.00	**2.84**	4.32	8.64	22.0	**2.54**
1426+015 (Mrk 1383)	21.2	1.09	1.19	**0.55**	5.27	18.6	4.07
1534+580 (Mrk 290)	22.2	1.99	**0.60**	**0.44**	1.37	6.68	6.85
1552+08	21.0	2.48	3.83	**0.65**	2.13	7.63	11.1
2041−109 (Mrk 509)	11.7	2.24	**0.66**	3.50	16.2	40.5	2.58
2209+185	2.37	0.74	0.69	**0.52**	**0.54**	0.71	1.48

[a] Values in bold face are models with lowest χ^2 for that AGN.

[b] For these blazars we assumed the nonstellar and power-law models are the same.

polarization was assumed equal to a constant of proportionality times the flux. For the dust hypotheses, the polarization was adjusted by a constant of proportionality times: λ^{-1}, λ^{-2}, or the wavelength dependence of the MRN dust mixture. We obtained least-squares fits of these polarization models to the observations by varying the constants of proportionality. The reduced χ^2 errors, between the different polarization hypothesis fits and the observations, are presented in Table 6. The polarimetry of all three blazars shows much better agreement with the predictions of the nonstellar/power-law models than with that of polarization from dust scattering.

Similarly, we investigated the polarization spectrum of Mrk 486, which Schmidt & Miller (1985) have shown rises from dust scattering. Through fits to the multiwavelength continuum we estimated the strengths of individual components in each waveband, and then predicted the resultant polarization spectrum for each hypothesis of the polarization's origin. We fit each polarization model to the observations and computed the χ^2 errors (Table 6). The model of MRN-type dust producing the polarization matches the shape of the observed polarization spectrum in Mrk 486 far better than the competing hypotheses.

5. DISCUSSION OF FITS

5.1. *Power-Law and Nonstellar Hypotheses*

The χ^2 values of the model fits for the remaining 14 objects are summarized in Table 6. For each object, the lowest χ^2 values of the seven models are highlighted in boldface. Some objects have more than one model with a low χ^2 value, and uncertainties in the data and models allow more than one model interpretation.

Our *UBVRI* polarimetry rules out the uniformly polarized power-law hypothesis with a slope steeper than −0.7 for all of the AGNs we measured, except for 0414−06, 1048−09, and 1254+047. The latter two were not model-fitted because their measured optical fluxes disagreed sharply with their ultraviolet fluxes. This disagreement is probably due to strong continuum variability between the dates of the optical and *IUE* spectroscopy. The polarized fluxes of the latter two objects appear to rise to longer wavelengths, consistent with production by a (nonthermal) polarized power-law component. In PG 1048−09 (3C 246), this is probably the signature of a "miniblazar" like the one detected in 3C 273 (Impey et al. 1989). The unusually large optical/UV variability we see in these three quasars is also consistent with the blazar interpretation. PG 1048−09 (3C 246) differs from classical "high-polarization quasars," such as PKS 0736+01 and PKS 1510−089 in Malkan & Moore (1986), in having a low ratio of core to lobe radio flux. PG 1254+047 is even less clearly related, since it is radio-quiet (Kellerman et al. 1989).

The increase in polarization to shorter wavelengths in all the other program objects prevents us from attributing it to any power law which is redder than the total spectrum. Thus any uniformly polarized power-law component would need to have an average slope flatter than −0.7, to avoid producing polarization percentages which increase to the red. In most of the AGNs, the increase in polarization to the blue is large enough that even a polarized flux (PF) proportional to $\nu^{-0.4}$ is ruled out (see Table 3). Jones & Stein (1987) have proposed that much of the optical continuum in radio-quiet, low-polarization quasars is due to nonthermal emission with a power-law slope of −0.5. For most of our objects the polarimetry appears to rule out the simplest version of this model, which attributes the power law to uniformly polarized synchrotron emission.

If any portion of the polarization were attributable to a red power-law component, our observations at the longest wavelengths set strict upper limits on the intrinsic polarization of the power law. For example, the power law typically produces one-quarter to half of the observed I flux. For observed polarizations of 0.3% at that wavelength, the power law cannot be more than 0.6 to 1.2% polarized. The polarization limits at 2.2 μm are even more restrictive, since the power law would usually produce nearly all of the flux at that wavelength.

The uniformly polarized nonstellar continuum hypothesis fits the data for 0414−06 (3C 110) with low signal-to-noise,

and possibly 1222+228. The nonsetllar continuum hypothesis predicts that the polarized flux should *decrease* with frequency, although not as sharply as the pure power-law hypothesis discussed above. All of the *other* 13 objects have higher polarized fluxes in the blue than predicted by the nonstellar model. These objects have excess polarized blue flux independent of whether or not the Balmer continuum/Fe II emission blend in the UV is polarized.

Antonucci has proposed that three luminous radio-loud quasars not included in this study (Ton 202, 3C 323.1, and 4C 34.47) have a constant wavelength-independent polarization arising from electron scattering of nuclear light. For these objects the contamination from starlight is negligible, but at wavelengths below 4000 Å the redshifted unpolarized Balmer emission dilutes the polarization. Although the optical spectropolarimetry covers a relatively narrow range of rest wavelengths (e.g., 6300–4300 Å), these radio-loud quasars would appear to best fit our nonstellar hypothesis. New near-IR polarimetry for Ton 202 and 3C 323.1 (Sitko & Zhu 1991) show polarizations of 1%–1.5% at 2 μm, similar to those measured in the optical. This is consistent with our interpretation of the near-infrared continuum as arising in the nucleus and hence experiencing the same scattering (by electrons?) as the optical. If the near-IR were thermal emission from hot dust grains in the BLR, it would be unpolarized (since the BLR emission is unpolarized). This implies that the near-IR polarized flux does not arise from hot dust in or beyond the BLR.

5.2. *Dust-scattering Hypotheses*

Most of the program objects have polarizations best modeled as arising from scattering off various types of dust grains. The observed polarized fluxes in several quasars (0134+329, 0711+458, 1004+130, 1426+015, 1534+580, 1535+547, 1552+08, and 2209+185) are most similar to predictions of the MRN dust model. The hypothesis that polarization increases as rapidly as the inverse square of the wavelength can be ruled out for every AGN in our sample except 0050+124 (I Zw 1). In fact, the only way that I Zw 1 could have polarization properties similar to the other dusty sources in this program, is in the unlikely event that we underestimated the amount of starlight contamination in the red by a factor of 3. Further, the dusty Markarian galaxies would also be subject to this error (since starlight in their spectra is probably of comparable importance), yet they do not show the same polarization behavior. This strong wavelength dependence of polarization from dust scattering is observed in the *IRAS*-selected dusty quasar 14026+4341, but is not expected to be common in UV-selected AGNs.

5.3. *The Thermal Component Hypothesis*

The thermal component model best fitted the polarization spectra of more objects than any other model except for MRN-type dust. The AGNs whose polarization spectra were best matched by the thermal hypothesis—1208+397 (NGC 4151), and 2041−109 (Mrk 509), and possibly 1415+253 (NGC 5548)—could be fitted with different levels of components so that the χ^2 values of the thermal hypothesis varied over a factor of 2. However, in all component fits, the χ^2 values of the thermal model were lower than the values of all other polarization hypotheses. In 0050+124 (I Zw 1), 0134+329 (3C 48), 0711+458 (Mrk 376), and 1535+547 (Mrk 486), different acceptable multicomponent fits gave χ^2 values for the thermal component hypothesis which differed by up to factors of 2, sometimes changing its relative ranking among hypotheses.

We also examined the uncertainties in our fitting procedure arising from different assumptions about the thermal component. We refitted the multiwavelength continua of nine of our program quasars by replacing the accretion disk model for the thermal component with a single one-temperature blackbody. The blackbody form is computationally simple and has some physical motivation. It could be a reasonable description of the spectrum of a geometrically thick radiation torus. These simple blackbodies lead to blue bumps with a flux which rises more sharply to the blue, and produce somewhat brighter "power-law" components with flatter slopes, than do the broader accretion disk spectra. In most cases, we found the blackbody spectrum gave rise to higher χ^2 values for the thermal component fit, than did the accretion disk model. Two exceptions are AGNs with the larger values of "*b*" in Table 3—PG 0050+124 (I Zw 1) and PG 1534+580 (Mrk 290), for which the steeply rising blackbody flux is a better match to the rising polarization in the blue.

We tried modifying the "power law" used in our fits to cut off exponentially above 1.1×10^{14} Hz. As described in Malkan (1989), this analytically simulates thermal infrared emission by a distribution of warm and hot dust grains. The principle effect is to require that the thermal component produces more of the flux in the red and visual wavebands. This results in a fit with a larger, cooler accretion disk, essentially the opposite of introducing the blackbody thermal component. As expected, none of the polarization model fits other than the power law and thermal component hypotheses are significantly affected by this assumed cutoff. In some cases, where the previous thermal fit had yielded the best χ^2, the change to an exponentially cutoff power law makes it significantly less good (e.g., 1208+397 [NGC 4151]). Conversely, if the thermal hypothesis had produced too strong a polarization increase to short wavelengths, it yields a better χ^2 if the power law is cut off, as in 1415+253 (NGC 5548).

Our conclusions are based primarily on polarimetry at wavelengths shortward of 0.8 μm. Since we are not certain of the physical nature of the infrared flux, there is a variant of the nonstellar hypothesis which can be difficult to distinguish from the thermal hypothesis. Suppose that there is no nonthermal "power-law" component, and that the near-IR flux is purely thermal emission from hot dust grains surrounding (but not immediately inside) the central nuclear continuum source. If the thermal infrared flux is unpolarized, all of the polarized flux would have to come from the remaining optical/UV component. If, as we suppose, this is identified with the accretion flow, then the conceptual difference between the nonstellar and thermal hypotheses would be blurred. Then the principal difference between the two hypotheses is whether or not the flux density of the optical/UV component drops at wavelengths beyond 0.8 μm. If the near-infrared continuum is thermal emission from dust, the optical/UV component is strong in the red; if the near-infrared is nonthermal, the optical/UV component must drop in the red (Malkan 1989). If the optical/UV component is indeed uniformly polarized, then the nonthermal infrared scenario would predict a sharper drop in polarization at long wavelengths than would the thermal infrared scenario. Sitko & Zhu's (1991) polarimetry does not favor either of these hypotheses, and distinguishing between them will require very accurate polarimetry extending from the visual into the near-infrared.

The thermal UV hypothesis (no. 6) requires that all the polarization originates in the blue/UV component. All other components are presumed to be unpolarized, and the ratio of measured polarization to the actual disk polarization equals the ratio of disk light to the total light. SMA measured the net polarization of the total optical flux for a large number of quasars. The different redshifts of objects in the SMA sample would be expected to cause the disk light from otherwise identical objects to produce different fractions of the observed optical light. If most of the polarization in this sample were produced by a uniformly polarized optically thick thermal component, one would then expect the average percentage of polarization to first increase with redshift. Since such an effect has not been seen, we can conclude that the uniformly polarized thermal component hypothesis alone cannot fully explain the polarization in most quasars.

Laor, Netzer, and Piran have calculated the polarization expected from thin disks with nonnegligible absorption opacity at optical wavelengths. As expected, the decrease in albedo at longer wavelengths in the disk atmosphere leads to significantly reduced polarization. At the shortest wavelengths (in the far-ultraviolet), the polarization is also decreased, by the differential rotation of the polarization vectors of light rays which pass near the black hole. This purely relativistic effect could also produce a detectable rotation in the plane of polarization, but only at the very shortest wavelengths, shorter than 1000 Å for most disks. There is no indication that our optical polarimetry has revealed such an effect, although *HST* UV polarimetry could be decisive.

In high-redshift quasars (like many in the SMA sample) the thermal component would be expected to produce up to 70% of the white light continuum. If these disks were flat and optically thick, their polarizations might be similar to the semi-infinite plane parallel slab calculations of Chandrasekhar (1960) and Angel (1969). Those calculations indicated that the polarization of edge-on disks of pure electron scattering could approach 11%. Some high-redshift quasars would then be expected to be observed with white-light polarizations of over 5% (Webb & Malkan 1986). That such high polarizations are not observed in normal quasars and Seyfert galaxies suggests the unobscured flat disk may be too simple a model. In the second paper in this series we calculate the polarizations that would be expected from different types of accretion flows in an attempt to put limits on possible disk models. Perhaps lower optical depths, high absorption coefficients, disk opening angles of 10° or more, or other observational selection effects are suppressing high polarizations.

5.4. *Correlation of Polarization Model Fits with Other Properties*

We searched for correlations between the models which best fit the observed polarization and other properties of the program AGNs (Table 7). Those objects which are *not* well fitted by dust polarization have lower average polarization, and perhaps higher Lyman-α:Hα ratios, and weaker Fe II line emission. One reasonable interpretation is that the dust-polarized quasars are also more likely to be reddened by the same dust grain scatterers. It appears that the dust-scattering mechanism is also more capable of producing large (1%–4%) polarizations, and that it also causes similar polarizations in the emission lines, which are, in contrast, unpolarized in AGNs polarized by another mechanism. AGNs with polarization best modeled as having a thermal origin, and which have measured Hα, NGC 4151 and Mrk 509, have very little Hα polarization. If confirmed, this potentially important correlation would lend credence to our modeling technique's ability to distinguish physical polarization mechanisms.

In the "dust-polarized" quasars, since the scatterers are evidently well outside the broad-line region, they could produce the observed polarization for a variety of primary continuum emission mechanisms. Our polarimetry does not uniquely distinguish these possible origins. For example, if the nuclear continuum were produced by intense starburst activity (rather than a nonstellar central engine; e.g., Terlevich et al. 1992), it would probably produce an MRN-dust polarization signature, if it produced any polarization at all. Nonetheless, we know that the continuum-producing region should be compact relative to the (nonspherical) distribution of dust grains, so that the position angle of polarization is independent of wavelength, as we observed.

TABLE 7

CORRELATIONS OF POLARIZATION WITH OTHER PROPERTIES OF AGNS

Object	Best-Fit *P* Model	White *P*	α(60:2.2 μm)	Lyα:Hα	Fe II:Hβ	Hα Polarized	$F_{6cm}:F_{4400Å}$	Optical Polarization P.A.	Optical Axis	Radio Axis	References
0050+124	Dust	0.61%	−1.1	1.25	2.8	...	0.33	8° ± 3°	110° ± 5°	...	1
0134+329	Dust	1.45	−1.5	0.11	2.2	...	...	160 ± 3	12 ± 1	...	...
0414−06	Ns	0.86	> −1.3	3:?	<0.5	...	...	145 ± 5	...	...	...
0711+458	Dust	4.37	−1.0	...	1.0	Yes	<6.	177	175	...	4, 5
1004+130	Dust	0.76	−1.0	...	...	...	228.	77 ± 8	125 ± 5	114° ± 5°	1
1114+445	Thermal/Dust	2.33	> −1.	Small	...	...	0.13	98 ± 3	96 ± 2	...	1
1208+397	Thermal	1.62	−1.0	1.36	0.15	No	0.96	88	26	...	2, 5
1222+228	PL/Ns	0.95	> −1.2	...	...	...	4.09	147 ± 8	...	...	1
1415+253	Thermal/IT	0.44	−1.2	...	0.38	No	0.60	33 ± 3	160, 110	...	5
1426+015	Dust	0.49	−0.9	...	...	...	0.28	58 ± 11	50 ± 10	50 ± 10	1
1534+580	Dust/Thermal	0.79	> −0.7	...	0.2:?	...	0.70	128 ± 6	50 ± 5	60 ± 5	1
1535+547	Dust	2.48	> −0.7	0.13[a]	0.9	Yes	0.14	133 ± 1	150 ± 5	120 ± 7	1, 3
1552+08	Dust	1.88	> −1.07	...	...	...	0.45	75 ± 3	...	...	1
2041−109	Thermal	0.87	−0.9	1.8	0.16	No	0.20	150 ± 2	70, 110	...	5
2209+185	Dust	1.21	> −0.9	...	...	...	141.	24 ± 7	90 ± 5	...	1

[a] Lyα is self-absorbed.

REFERENCES.—(1) Berriman et al. 1990. (2) Schmidt & Miller 1980. (3) Schmidt & Miller 1985. (4) Martin et al. 1982 (5) Thompson & Martin 1988.

Stockman, Angel, & Miley (1979) found a mild tendency for radio-loud quasars to have radio structures aligned with the E-vector of their optical polarizations. However, no such alignment has been reported in Seyfert galaxies (Martin et al. 1983) or in radio-weak quasars (Berriman et al. 1990). Since most of our sample AGNs are radio-weak, it is not surprising that their polarization and radio position angles, listed in Table 7, are not generally aligned. Even the radio-loud quasar 1004+130 (4C 13.41) shows no alignment, and our genralizations about polarization mechanisms may not apply to that minority of quasars which are radio-loud and show radio/polarization alignment.

Of course, it is more difficult with a small sample such as ours to establish a positive statistical *alignment* of axes. Table 7 also compares the optical polarization position angles with the major axes of the host galaxies. Four of the AGNs with polarizations which can be adequately described by dust scattering have electric vector position angles lying within about 20° of the major axis of their respective host galaxies (1114+445, Mrk 376, 486, and 1383). This could be taken as consistent with the idea that dust scattering in the host galaxy is important in these cases, although hardly statistically decisive.

5.5. *Future Observations*

The degree of confidence with which the various polarization hypotheses can be accepted or rejected is, of course, a very strong function of the signal-to-noise ratios of the polarimetry—the leading uncertainty in this study. Further gains could also be made by extending the spectral coverage. The percentage differences in polarized flux between the competing hypotheses grow proportionally to the wavelength baseline. If high S/N polarimetry can be obtained in the 1–2 μm region, any remaining ambiguities between the power-law and thermal hypotheses, for example, can be resolved decisively. Since the polarizations are usually low at I, the near-IR polarimetry will need precisions of 0.1% or better, which may be marginally feasible for the brightest quasars.

Discrimination between the dust (MRN) and blue thermal component models can best be made with polarimetry in the ultraviolet. This extension to shorter wavelengths can be made with the *HST* Faint Object Spectrometer in spectropolarimetry mode.

Our selection in this study (of the higher polarization normal quasars from previous white-light surveys) may have biased the proportion of quasars for which different polarization models provided the best fits. Our sample objects fitted best by the thermal model have lower intrinsic polarizations than the objects best fitted by the dust models. Therefore, a wider sample of normal quasars with lower average polarization might have a larger percentage of objects with polarization fitted best by the thermal model.

Although difficult to obtain, repeated *UBVRI* polarimetry with high signal-to-noise ratios would be valuable in the search for QSOs with variable continua. If the polarization is due to scattering (MRN, λ^{-1}, λ^{-2}, or Ns hypotheses), or interstellar transmission (IT hypothesis), no change in the percentage of polarized light is expected when the continuum changes. We assume that the polarizers (dust grains or free electrons) are far enough away from the central continuum that their geometry does not vary, and that dilution from starlight is negligible, or has been corrected. If, however, the polarization arises from one component which does not contribute equally to the continuum at all wavelengths, wavelength-dependent polarization changes would be expected. For example, if a power-law component brightens, it would increase the polarization most at the longer wavelengths. (This effect from a "mini-blazar" has been seen in 3C 273, and should be sought in 3C 246). If the polarization arises from a "Big Blue Bump" (thermal hypothesis), then when the continuum brightens (presumably due to increasing flux from the thermal component), the blue polarization would generally rise more than that at longer wavelengths. The simplest signature would be a thermal component whose flux varies, but whose percentage intrinsic polarization (after model decomposition) does not change significantly.

6. CONCLUSIONS ABOUT SOURCES OF POLARIZATION IN AGNS

We have analyzed the wavelength dependence of polarization in more than 15 normal quasars and Seyfert I galaxies to test various hypotheses for its origin. The polarization of the nuclear continuum in most of these AGNs is not wavelength-independent, but increases to shorter wavelengths. In nearly every case, the polarization position angle vector appears fixed, suggesting a single polarizing mechanism (or possibly multiple mechanisms sharing a special geometry).

Our *UBVRI* polarimetry rules out the uniformly polarized power-law hypothesis with a slope steeper than −0.7 for all of the AGNs we measured, except for 0414−06, 1048−09, and 1254+047. The latter two objects have polarizations which appear to rise to longer wavelengths, consistent with production by a (nonthermal) polarized power-law component. In PG 1048−09 (3C 246), this is probably the signature of a "mini-blazar" like the one detected in 3C 273 (Impey et al. 1989). The large optical/UV variability we see in these three quasars is also consistent with the blazar interpretation. The radio-loud quasar, 3C 246 differs from classical "High Polarization Quasars," such as PKS 0736+01 and PKS 1510−089, in having a low ratio of core to lobe radio flux. PG 1254+047 is even less clearly related, since it is radio-quiet (Kellerman et al. 1989).

To test the proposed hypotheses for the physical origin of the polarization we have separated the various emission components believed to produce the multiwavelength continuum in our program AGNs. We used these spectral decompositions to compare our polarimetry to the predictions of seven polarization hypotheses, and reached the following conclusions. In several of our normal quasars and Seyfert I galaxies, the continuum polarizations were best modeled as scattering from a nonspherical distribution of dust grains, with polarization properties described roughly by the MRN mixture. The existence of this dust scattering should be confirmed by the polarization it imparts to the broad emission lines, at the same level and position angle as the underlying continuum.

For several AGNs, the observed polarization increases more steeply into the blue than any other continuum component except the thermal spectrum. The polarization in these objects most nearly resembles a constant percentage polarization of the continuum of a simple accretion disk model. If the broad emission lines (Hα being the easiest to observe) are unpolarized, this would be further consistent with the thermal hypothesis. If the BLR emission shares the same polarization as the surrounding continuum, the dust-scattering hypothesis would be favored. As we would have predicted, the broad lines in the best measured thermal fit candidates, Mrk 509 and NGC

5548, are observed to be virtually unpolarized. Our study predicts that when spectropolarimetry is obtained for most of the other AGNs in this sample, it will reveal broad lines polarized the same as the continuum.

We have shown that the power-law, nonstellar continuum, and interstellar transmission hypotheses fail to reproduce the polarization spectra of most of the normal quasars and Seyfert I galaxies in our program. Dust models best represent the polarization spectra of many of these AGNs. Many of these same objects are independently known to be less blue in color, to have higher white-light polarized fluxes, and to have polarized emission lines. We find another group of AGNs whose polarization spectra are best represented as being proportional to a blue thermal component. Many of these same objects are independently known to be bluer in color, to have smaller white-light polarizations, and to have unpolarized emission lines. These data are consistent with all LPQs having blue thermal components which are uniformly polarized at low levels, and many objects having an additional, comparable, or larger (not necessarily aligned) component of dust polarization. This suggests the polarization characteristics of the blue bump might best be studied in objects with *low* white-light polarization, in dust-free objects with *unpolarized* emission lines, and at high signal-to-noise, extending as far as possible into the ultraviolet.

Better tests of the scattering and thermal hypotheses clearly require more wavelength-dependent polarimetry with signal to noise ratios of 8–10, and the maximum possible wavelength baseline. Most of the models are best tested by the polarizations measured at the shortest and longest wavelengths. High-quality polarimetry at 2 μm and in the ultraviolet will prove an extremely powerful means of revealing the origins of polarization in AGNs.

We thank S. Tapia for assistance with the MINIPOL observations and acknowledge support in part by a NASA research grant NAG 5-1449.

REFERENCES

Allan, P., & Keel, W. 1993, in preparation
Angel, J. R. P. 1969, ApJ, 158, 219
Antonucci, R. R. J. 1984, ApJ, 278, 499
———. 1988, in Supermassive Black Holes, ed. M. Kafatos (Cambridge: Cambridge Univ. Press), 26
Antonucci, R. R. J., & Miller, J. S. 1985, ApJ, 297, 621
Berriman, G. 1989, ApJ, 345, 713
Berriman, G., Schmidt, G. D., West, S. C., & Stockman, H. S. 1990, ApJS, 74, 869
Burstein, D., & Heiles, C. 1978, ApJ, 225, 40
Chandrasekhar, S. 1960, Radiative Transfer (New York: Dover)
Cutri, R. M., Wicniewski, W. Z., Rieke, G., & Lebofsky, M. J. 1985, ApJ, 296, 423
de Bruyn, A., & Sargent, W. 1978, AJ, 83, 1257
Edelson, R., & Malkan, M. 1986, ApJ, 308, 59
Hutchings, J. B., Crampton, D., Campbell, B., Duncan, D., & Glendenning, B. 1984, ApJS, 55, 319
Impey, C. D. 1987, in Superluminal Radio Sources, ed. J. Zensus & T. Pearson (Cambridge: Cambridge Univ. Press), 233
Impey, C. D., Malkan, M. A., & Tapia, S. 1989, ApJ, 347, 96
Impey, C. D., & Tapia, S. 1989, ApJ, 354, 124
Jones, T. W., & Stein, W. A. 1987, ApJ, 320, L1
Kellermann, K. I., Sramek, R., Schmidt, M., Shaffer, D., & Green, R. 1989, AJ, 98, 1195
Laor, A., Netzer, H., & Piran, T. 1990, MNRAS, 242, 560
Malkan, M. 1983, ApJ, 268, 582
———. 1989, in Theory of Accretion Disks, ed. F. Meyer et al. (Dordrecht: Kluwer), 19
Malkan, M., & Filippenko, A. 1983, ApJ, 275, 477
Malkan, M., & Moore, R. 1986, ApJ, 300, 216
Malkan, M., & Sargent, W. L. W. 1982, ApJ, 254, 22
Martin, P., Stockman, H. S., Angel, J. R. P., Maza, J., & Beaver, E. A. 1982, ApJ, 255, 65
Martin, P., Thompson, I., Maza, J., & Angel, J. R. P. 1983, ApJ, 266, 470
Mathis, J. S., Rumpl, W. M., & Nordsieck, K. H. 1977, ApJ, 217, 425 (MRN)
Neugebauer, G., Oke, J. B., Becklin, E. E., & Mathews, K. 1979, ApJ, 230, 79
Neugebauer, G., Green, R. F., Mathews, K., Schmidt, M., Soifer, B. T., & Bennet, J. 1987, ApJS, 63, 615
Neugebauer, G., Mathews, K., Soifer, B., & Elias, J. 1985, ApJ, 298, 275
Schmidt, G., & Miller, J. 1980, ApJ, 240, 759
———. 1985, ApJ, 290, 517
Serkowski, K., Mathewson, D. S., & Ford, V. L. 1975, AJ, 196, 261
Sitko, M. L., & Zhu, Y. 1991, ApJ, 369, 106
Smith, P. S., Balonek, T. J., Elston, R., & Heckert, P. A. 1987, ApJS, 64, 459
Stockman, H. S., Angel, J. R. P., & Miley, G. K. 1979, ApJ, 227, L55
Stockman, H. S., Moore, R. L., & Angel, J. R. P. 1984, ApJ, 279, 485 (SMA)
Sun, W. H., & Malkan, M. 1989, ApJ, 346, 68
Terlevich, R., Tenorio-Tagle, G., Franco, J., & Melnick, J. 1992, MNRAS, 255, 713
Thompson, I. B., Landstreet, J. D., Angel, J. R. P., Stockman, H. S., Woolf, N. J., Martin, P. G., Maza, J., & Beaver, E. A. 1979, ApJ, 229, 909
Thompson, I. B., & Martin, P. G. 1988, ApJ, 330, 121
Turner, T. J., & Pounds, K. A. 1989, MNRAS, 240, 833
Wardle, J. F. C., & Kronberg, P. P. 1974, ApJ, 194, 249
Webb, W., & Malkan, M. 1986, in The Physics of Accretion onto Compact Objects, ed. K. O. Mason, M. G. Watson, & N. E. White (Berlin: Springer), 15
White, R. L. 1979, ApJ, 229, 954
Wills, B. J., et al. 1989, in Active Galactic Nuclei, ed. D. E. Osterbrock & J. S. Miller (Dordrecht: Kluwer), 325